

Time-resolved velocity and concentration measurements in variable-viscosity turbulent jet flow

Benoît Talbot · Nicolas Mazellier · Bruno Renou ·
Luminita Danaila · Mourad Abdelkrim Boukhalfa

Received: 1 October 2008 / Revised: 31 July 2009 / Accepted: 4 August 2009 / Published online: 22 August 2009
© Springer-Verlag 2009

Abstract This paper addresses the ability to reliably measure the fluctuating velocity field in variable-viscosity flows (herein, a propane–air mixture), using hot-wire anemometry. Because the latter is sensitive to both velocity and concentration fluctuations, the instantaneous concentration field also needs to be inferred experimentally. To overcome this difficulty, we show that the hot-wire response becomes insensitive to the concentration of the field, when a small amount of neon is added to the air. In this way, velocity measurements can be made independently of the concentration field. Although not necessary to velocity measurements, Rayleigh light-scattering technique is also used to infer the local (fluctuating) concentration, and, therefore, the viscosity of the fluid. Velocity and concentration measurements are performed in a turbulent propane jet discharging into an air–neon co-flow, for which the density and viscosity ratios are 1.52 and 1/5.5, respectively. The Reynolds number (based on injection diameter and velocity) is 15400. These measurements are first validated: the axial decay of the mean velocity and concentration, as well as the lateral mean and RMS profiles of velocity and concentration, is in full agreement with the existing literature. The variable-viscosity flow along the axis of the round jet is then characterized and compared with a turbulent air jet discharging into still air, for which the Reynolds number (based on injection diameter and velocity) is 5400. Both flows have the same initial jet momentum. As mixing with the viscous co-flow is

enhanced with increasing downstream position, the viscosity of the fluid increases rapidly for the case of the propane jet. In comparison with the air jet, the propane jet exhibits: (1) a lower local Reynolds number based on the Taylor microscale (by a factor of four); (2) a reduced range of scales present in the flow; (3) the isotropic form of the mean energy dissipation rate is first more enhanced and then drastically diminishes and (4) a progressively increasing local Schmidt number (from 1.36 to 7.5) for increasing downstream positions. Therefore, the scalar spectra exhibit an increasingly prominent Batchelor regime with $a \sim k^{-1}$ scaling law. The experimental technique developed herein provides a reliable method for the study of variable-viscosity flows.

1 Introduction

A variety of engineering applications require mixing of two fluids at rate as high as possible. In reactive flows, molecular mixing of the fuel and oxidizer is a necessary precursor to the chemical reaction. In this context, a correct understanding of the interaction between the scalar and velocity fields is crucial, especially in complex fluids and flows (Nelkin 2000; Shraiman and Siggia 2000). In the case of the non-premixed combustion regime, both reactants (fuel and oxidizer) are generally injected through two distinct channels and merge in the near wake of a splitter plate separating these channels. This merging is followed by a non-reacting, isothermal, partially premixed region, where both reactants are mixed together. In the case of the lifted flame regime, the mixing layer that develops upstream of the flame front occurs at a relatively constant, ambient temperature, so that the chemical reaction can be considered to be frozen (Fernandez-Tarrazo et al. 2006).

B. Talbot (✉) · N. Mazellier · B. Renou · L. Danaila ·
M. A. Boukhalfa
UMR 6614 CORIA, Université et INSA de Rouen,
76801 Saint Etienne du Rouvray, France
e-mail: benoit.talbot@coria.fr

The non-reacting partially premixed region is crucial to the stabilization of the flame located just downstream of it. In particular, a strong vortex/flame interaction is generated when the flow field in this region is turbulent. Here, the flame front may be either swept or quenched (Hermanns et al. 2007), depending on the characteristic time scales of chemical reactions and the turbulence.

Therefore, the partially premixed region is isothermal, non-reacting flow and is relevant to the understanding of non-premixed combustion stabilization. Moreover, the study of isothermal mixing of reactants is also representative of any transient process (ignition, re-ignition, stabilization behind holders). To conclude, understanding isothermal non-reacting flows is an important step in characterizing non-premixed reactive flows. Although simpler than the latter, isothermal non-reactive flows involve fluids with variable density and viscosity. The focus of this paper is on isothermal flow, where two gases of different densities and viscosities are mixed.

Some questions pertaining to the mixing of scalars in turbulent flow have been addressed by numerical simulations, adding a significant insight into the statistics of the small-scale scalar field (Antonia and Orlandi 2003; Boersma et al. 1998; Brethouwer et al. 2003; Lubbers et al. 2001). However, most of the simulations treated the mixing of fluids of the same viscosity, which is not representative of most industrial applications. Some examples are propane–air, butane–air and hydrogen–air mixtures, for which the viscosity ratios are 1/3.4, 1/5.2 and 1/0.15, respectively.

Experimental studies have also furthered our understanding of variable density/viscosity flows. Although a large amount of experimental data exists for separate measurements of either velocity or concentration in turbulent gaseous flows, simultaneous time-resolved measurements are much less common. Several coupling techniques have been developed such as high speed Particle Image Velocimetry/Planar Laser Induced Fluorescence (Feng et al. 2007; Su and Mungal 2004). However, these techniques require a complex experimental arrangement and are limited by the maximum frequency of the pulsed lasers (~ 5 kHz) and by their low resolution in space/time. These limitations are significant in the near-field region of the flow, where other problems such as the restricted size of the volume to be investigated, or inhomogeneous seeding, are common.

Single-point, time-resolved (and seeding-free) coupled techniques (for the scalar and velocity) are, therefore, more adapted for the investigation of the near-field region. Different experimental techniques for simultaneous, one-point, time-resolved scalar and velocity measurements (with or without seeding) were developed. Several authors (Lemoiné et al. 1999; Miller and Dimotakis 1996) addressed the issue of measuring scalar and velocity fields in liquids.

Nevertheless, major drawbacks of these techniques can be argued and include:

- Highly intrusive sensors (Era 1993);
- Techniques limited to inert gaseous mixtures only (Chassaing 1979; Sakai et al. 2001);
- High cross dependence of concentration/velocity measurements in both non-reactive gaseous mixtures (Chassaing 1979; Sakai et al. 2001; Way and Libby 1971) and reactive ones (Dibble et al. 1987).

As far as non-intrusive techniques are concerned, only one attempt has been proposed [by Pitts et al. (1983)] for local simultaneous time-resolved measurements of concentration and velocity, combining one-point Rayleigh light-scattering (RLS) and hot-wire anemometry (HWA). Methane and propane jets were studied to validate their technique. Despite the potential of this approach, the authors discussed the difficulty to accurately determine the fluid velocity, due to the sensitivity of the hot wire to both velocity and concentration. In this work, we propose a new, more reliable technique inspired by (Pitts et al. 1983), allowing the velocity field to be measured independently of the scalar field. The technique we develop herein is based on the addition of a neutral gas (in a controlled proportion) to the air.

The paper is organized as follows. In Sect. 2, we first review the basic principles of HWA and RLS and highlight the major difficulties encountered when these techniques are coupled. Then, we present the innovative technique that we have developed. The experimental setup and measurement conditions are described in Sect. 3. A validation of our new technique with the existing literature is given in Sect. 4. A discussion of the main results using our new technique for a propane jet discharging into a mixture of air and neon is presented in Sect. 5. The effects of viscosity gradients are highlighted by comparing our flow with an air jet discharging into a stagnant air medium at the same initial jet momentum. Lastly, conclusions are provided in Sect. 6.

2 Theory of hot-wire anemometry (HWA) and Rayleigh light scattering (RLS) in multi-component mixtures

2.1 The “Constant-shift” method

The experimental arrangement of the coupling technique is the same as that proposed by Pitts et al. (1983). HWA and RLS are coupled to measure simultaneously scalar and velocity fluctuations. Figure 1 shows a sketch of the experimental setup used in the present work. The hot-wire probe is located at a distance of 800 μm downstream of the

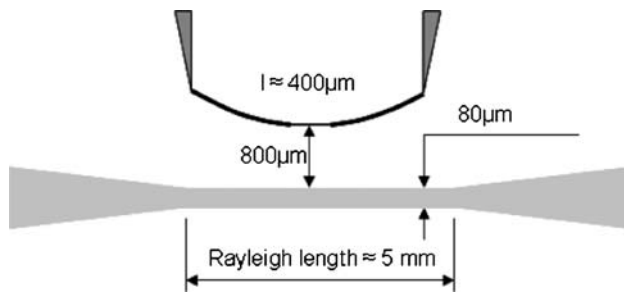


Fig. 1 Arrangement of HWA and RLS coupling technique. The hot-wire probe is positioned at 800 μm downstream the focused laser beam (80 μm diameter)

Rayleigh probe volume. This distance cannot be reduced, because of light interference between the laser beam and the hot-wire prongs.

The local concentration fluctuation can be directly determined by RLS. In mono-component gases, the hot wire is sensitive to the cooling due to the fluid convection around the probe. Under such conditions, the signal recorded by the hot-wire anemometer is directly related to the local, and almost instantaneous, velocity fluctuations.

However, in multi-component gases, the hot wire is sensitive to both the local velocity and the local fluid properties, i.e. the local concentration. It is, therefore, essential to know exactly these local properties at the wire location, in order to extract the velocity signal from the hot-wire signal. Pitts et al. (1983) proposed to apply a constant temporal shift δt between the Rayleigh signal and the hot-wire signal and, therefore, to “translate” the concentration signal at the hot-wire point, by taking $\delta t \equiv \delta Z / \langle U \rangle$, where δZ is the spatial separation between the Rayleigh and the hot-wire probes, and $\langle U \rangle$ is the axial mean velocity at the Rayleigh probe location. As only δZ is known and the velocity $\langle U \rangle$ is unknown *a priori*, the value of the constant shift cannot be properly chosen. Consequently, a Taylor hypothesis cannot be formulated, and the high-order moments velocity statistics cannot be determined with accuracy because of their very high sensitivity to δt . This *a priori* problem can be overcome by adding a precise quantity of an inert gas to the air flow at constant mass flow rate. Herein, neon is the inert gas chosen.

2.2 The new HWA method using neon doping

The method we have developed leads to a constant heat transfer between the resulting mixture at the hot-wire location, thus eliminating the sensitivity of the hot-wire signal to the concentration of the mixture.

The thermal equilibrium of a heated cylindrical wire is given by the following equation:

$$i^2 R_w = \pi l \lambda [T_w - T_o] \text{Nu}, \quad (1)$$

where i denotes the electric heating current, R_w is the electrical resistance of the hot wire, l is the length of the wire, λ is the thermal conductivity of the gas, T_w and T_o are the temperatures of the wire and the air surrounding the wire, respectively, and ‘Nu’ is the Nusselt number (defined as $\text{Nu} = hd/\lambda$, where d is the wire diameter and h is the convective heat transfer coefficient). The temperature dependence of R_w may be expressed as follows:

$$R_w = R_o \{1 + b[T_w - T_o]\} = R_o \{1 + bT_o \alpha\}, \quad (2)$$

where R_o is the electrical resistance of the hot wire at ambient temperature T_o , and $\alpha = [T_w - T_o]/T_o$ is the temperature overheat ratio. The constant coefficient b is 0.0019 K^{-1} for Pt/Rh 90/10% used herein. Moreover, the following relation holds, for the electrical bridge of the anemometer

$$i^2 R_w = E_{\text{out}}^2 R_w / [R_b + R_a]^2, \quad (3)$$

where R_a is the electrical resistance of the probe leg (50 Ω), and R_b is the adjustable resistance of the Wheatstone bridge. Several expressions had been proposed for the Nusselt number, but no valid expression is available for any fuel–air mixture (Pitts and McCaffrey 1986). Despite of this remark, we further use here the following correlation for a binary gas mixture valid for $0.02 < Re = Ud/\nu < 44$ (Wu and Libby 1971):

$$\text{Nu}_c = [T_m/T_o]^{0.17} \times \left\{ 0.24 [Pr_1/Pr_2]^{0.20} + 0.56 [Pr_1/Pr_2]^{0.33} Re^{0.45} \right\}, \quad (4)$$

where Pr_1/Pr_2 is the ratio of the Prandtl numbers of the two investigated gases at the mean film temperature T_m

$$T_m = [T_w + T_o]/2 = T_o/2[\alpha + 2]. \quad (5)$$

By combining Eqs. 1–5, the voltage E_{out} can be expressed as

$$E_{\text{out}}^2 = \pi l \lambda \alpha T_o [(\alpha + 2)/2]^{0.17} \left\{ 0.24 [Pr_1/Pr_2]^{0.20} + 0.56 [Pr_1/Pr_2]^{0.33} [Ud/\nu]^{0.45} \right\} \times \left\{ [R_b^2 + 2R_b R_a + R_a^2] / [R_o(1 + bT_o \alpha)] \right\} \quad (6)$$

The validity of Eq. 6 is bounded by rare gas effects and natural convection at very low Re (< 0.02) and by vortex shedding effects at $Re = 44$. Equation 6 can be refined by taking into account the rare gas effects. Several studies of rare gases (Baccaglioni et al. 1969; Wu and Libby 1971) allowed for corrections of Nu, attributed to the thermal slip parameter β_{mix} , defined as

$$1/\text{Nu}_\infty - 1/\text{Nu}_c = \beta_{\text{mix}}/2, \quad (7)$$

where the subscript c refers to a continuum Nusselt number (i.e. in the absence of rarefied effects), and the subscript ∞ refers to the Nusselt number for a wire of infinite length, i.e. with no end losses in the presence of rarefied effects. A “heuristic mixture rule” has been given for the determination of the coefficient β_{mix} for mixtures. This rule is based on simple molar averaging (Baccaglioni et al. 1969):

$$\beta_{\text{mix}} \approx \sum \chi_i \beta_i, \quad (8)$$

where χ_i and β_i refer, respectively, to the molar fraction and thermal slip parameter of each component of the gas mixture. Introducing Eqs. 7 and 8 into Eq. 6 provides the final expression:

$$E_{\text{out}}^2 = \pi l \lambda \alpha T_o [(\alpha + 2)/2]^{0.17} \left\{ 1 / \left\{ 0.24 [Pr_1/Pr_2]^{0.20} + 0.56 [Pr_1/Pr_2]^{0.33} [Ud/\nu]^{0.45} \right\} + \beta_{\text{mix}}/2 \right\}^{-1} \times \left\{ [R_b^2 + 2R_b R_a + R_a^2] / [R_o(1 + bT_o\alpha)] \right\}. \quad (9)$$

By neglecting the Prandtl dependence (the Prandtl numbers are very close to unity, see Table 1), it follows from Eq. 9 that for a given HWA system (i.e. for fixed d , l , R_a , R_b , R_o , b) and for a given environment (i.e. T_o is fixed), E_{out} only depends on the following parameters: the fluid velocity U , the physical properties of the fluid (the thermal conductivity λ , the kinematic viscosity ν and the thermal slip parameter β_{mix}) and the overheat ratio α . If the overheat ratio is kept constant, Eq. 9 can be written as a function of the previously mentioned parameters governing the voltage drop across the wire, viz.

$$E_{\text{out}}^2 = A_o \lambda \left\{ 1 / [B_o + B_1 (U/\nu)^{0.45}] + \beta_{\text{mix}}/2 \right\}^{-1}, \quad (10)$$

where A_o , B_o and B_1 are constants that could be determined from Eq. 9 in a straightforward manner. Equation 10 shows that the voltage drop across the wire depends non-linearly on the velocity. Let us now apply these observations to the particular mixing under study (propane–air), with different mixing fractions and by adding different proportions of neon to the air.

Figure 2 (left) shows the computation of Eq. 10 as a function of the velocity, which ranges between 0 and 15 m s⁻¹, for (1) pure Propane, (2) pure Air, (3) a mixture

composed of 30% Air + 70% Neon in mass fractions (named “oxidizer”) and (4) a mixture composed of 50% Propane and 50% of “oxidizer” in mass fractions (named “50%”). The analytical curves are calculated with the following operating parameters: $\alpha = 1.067$, $l = 400 \mu\text{m}$, $d = 2.5 \mu\text{m}$, $R_o = 4.14 \Omega$, $R_a = 50 \Omega$, $R_b = 6.62 \Omega$, $b = 0.0019 \text{ K}^{-1}$, $T_o = 296 \text{ K}$. The physical fluid properties (λ , ν , β) of each pure gas are evaluated at the film temperature $T_m \approx 500 \text{ K}$, using the gases theory (Hirschfelder et al. 1966; Warnatz 1981) (the latter being very nearly equal to the mean temperature between the ambient and the wire temperature $T_w \approx 612 \text{ K}$). These physical properties are summarized in Tables 1 and 2.

Adding neon to the propane–air mixture results in the hot-wire response curves that closely follow each other, for any propane mass fraction varying between 0 and 100%.

Nevertheless, due to the non-linear dependence of Eq. 10 on the velocity, all the curves are not exactly superposed. Their intersection is at a unique velocity $U = 11.5 \text{ m s}^{-1}$. At this particular point, the error on velocity is exactly zero whatever the calibration curve considered for the hot-wire post-treatment. The benefit of adding neon is also illustrated on the same Fig. 2 (left) by the vertical arrows. The first two (from left to right) bound on the abscissa the minimum and maximum velocities of the fluid (20% variations around the mean value of 1.5 m s⁻¹), whereas the first and the third arrows bound a much larger domain of velocity (ranging from 1.5 to 7 m s⁻¹), thus emphasizing the tremendous velocity error that would have been made without adding neon.

We choose the curve corresponding to the mixture composed of 50% Propane and 50% “oxidizer” as the reference calibration curve for all the other mixtures that contain propane (ranging from 0 to 100%). The velocity corresponding to this 50% reference curve will be considered in the following as a “calibration” noted U_{cal} . Furthermore, an analysis of the induced error on the velocity, when the local and instantaneous fluid composition is different from that of 50%, is in order.

Figure 2 (right) shows the relative error $(U - U_{\text{cal}})/U_{\text{cal}}$ on estimating the velocity in this mixture of gases, in the range 0–15 m s⁻¹, while the real concentration of the propane differs from the value of 50%. Indeed, for a

Table 1 Physical properties of pure gases at the ambient ($T \approx 300 \text{ K}$) and at the film temperature ($T \approx 500 \text{ K}$)

	λ (300/500 K) in $\text{W m}^{-1} \text{ K}^{-1}$ From (Lide 2007)	ν (300/500 K) in $\text{m}^2 \text{ s}^{-1}$ From (Lide 2007)	Pr (300/500 K) From (Lide 2007)	β From (Baccaglioni et al. 1969)
Air	0.0258/0.0385	$16.04 \times 10^{-6}/38.94 \times 10^{-6}$	0.71/0.70	0.85
Propane	0.0180/0.0455	$4.60 \times 10^{-6}/12.69 \times 10^{-6}$	0.79/0.75	0.85
Neon	0.0498/0.0699	$28.66 \times 10^{-6}/63.38 \times 10^{-6}$	0.70/0.69	0.093

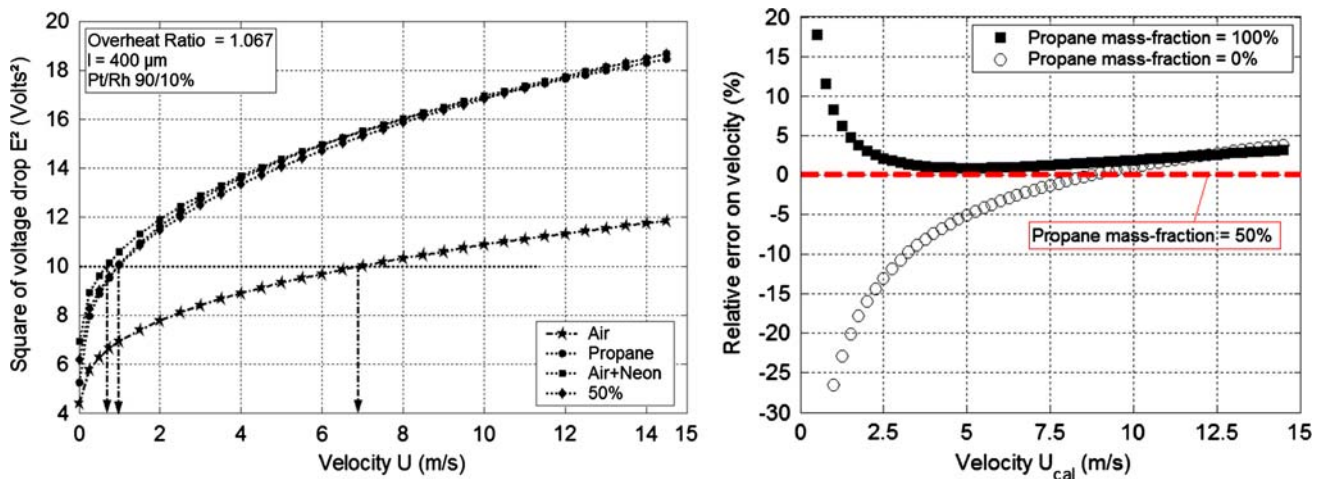


Fig. 2 Square of voltage drop across the hot wire, obtained from Eq. 9 (left) and corresponding relative error on velocity $(U - U_{cal})/U_{cal}$, (right)

Table 2 Physical properties of gas mixtures at the film temperature ($T \approx 500$ K) estimated from (Hirschfelder et al. 1966; Lide 2007)

	λ (500 K) in $\text{W m}^{-1} \text{K}^{-1}$	ν (500 K) in $\text{m}^2 \text{s}^{-1}$	β
Air–70% Neon	0.0570	60.75×10^{-6}	0.27
50% (Air–70% Neon)/50% Propane	0.0504	42.32×10^{-6}	0.20

concentration of 100% propane into the gas mixture, $(U_{100\%} - U_{cal})/U_{cal}$ is less than 5% between 1.4 and 15 m s^{-1} (Fig. 2, right). When a fluid particle composed of 0% propane comes around the hot wire, $(U_{0\%} - U_{cal})/U_{cal}$ reaches 20%. This error corresponds to the lowest velocity measurements, i.e. for $U_{cal} = 1.5 \text{ m s}^{-1}$. Obviously, the error is zero for a velocity measurement in a mixture composed of 50% mass fraction of propane (dashed-line in Fig. 2, right).

After this analytical investigation, we turn our attention to the experimental study of the velocity field with the HWA, for the four mixtures (1)–(4) already considered for the analytical study. The corresponding experimental curves are plotted on Fig. 3 (left). The global shapes of the curves are quite close to the analytical ones. Nevertheless, we can note a significant difference between the absolute level of the experimental and the analytical curves. This result is attributed to the uncertainties (of fluid physical properties or of conduction heat transfer) and to Eq. 4 that is not exactly adapted for propane–(air–neon) mixture. Figure 3 (right) shows the experimental relative error on the velocity in this mixture of gases, in the range 0–9.7 m s^{-1} , by using the 50% calibration curve for providing a velocity reference noted $\langle U_{cal} \rangle$ here (note that we use the time-averaged values because of the fluctuating velocity field in the experiment). For 100% mass fraction of propane, $(U_{100\%} - \langle U_{cal} \rangle)/\langle U_{cal} \rangle$ varies from +10 to

–12.5% in the range of 1.5–9.7 m s^{-1} , which corresponds to the velocity range of our study (see Table 4). For 0% mass fraction of propane, $(U_{0\%} - \langle U_{cal} \rangle)/\langle U_{cal} \rangle$ falls down from 0 to +2.5% for the same velocity range.

For the propane jet discharging in air–neon surroundings, particular values of propane mass fraction are illustrative for the mixing on the jet axis. We select seven of them, and the corresponding errors on mean velocity values are plotted on Fig. 3 (right), with red diamonds. Each point is associated to a specific position of measurement. Consequently, each point corresponds to a specific propane mass fraction given in Table 4. The errors on the mean velocity do not exceed –5.5% for the highest velocity measured in this study, which is $\langle U \rangle = 9.7 \text{ m s}^{-1}$. For this particular position, the probability density function of velocity field is Gaussian. The error on the fluctuating velocity is <5% ($1\sigma = 68\%$), <8% ($2\sigma = 95\%$) and <15% ($3\sigma = 99\%$), where σ refers to the standard deviation of the concentration (provided in Table 4). As far as the fluctuations around $\langle U \rangle$ are concerned, these are limited by

- $U = 0$, in which case they correspond to stagnating blobs of fluid that are associated to 0% propane (their origin is in the co-flow), and for which the relative error is –10%;
- $U \sim 10 \text{ m s}^{-1}$, in which case they correspond to rapid blobs of fluid associated to 100% propane (their origin is in the propane jet) and for which the maximum error is +2.5%.

Therefore, the maximal errors for fluctuating velocity field range from –10 to +15.5%, with a maximal relative error of 15%. However, note that this maximal relative error is reached for the maximal velocity of the flow and maximal scalar fluctuations (3 standard deviations of the scalar), which are very rare events.

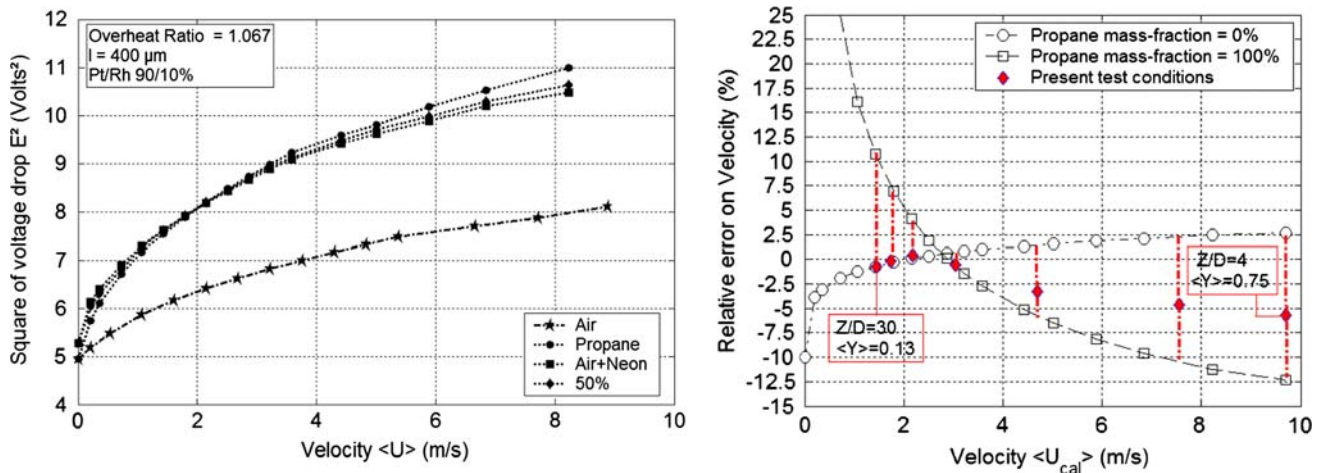


Fig. 3 Square of voltage drop across the hot wire obtained experimentally (left), and the corresponding error on velocity (right). The red points correspond to the relative error made for several conditions

As a conclusion of this part, we have developed a new technique for measuring velocity fluctuations in a propane–air mixture, independently of the local concentration measurement. This technique could *a priori* be extended in other different composition mixtures. In Sect. 4, we focus on the further validation of our technique, and in Sect. 5 we focus on new results. In the following, we remind some fundamentals of RLS. Although not anymore indispensable for the velocity measurement, RLS is, however, necessary for determining the propane mass fraction in the flow, and, therefore, the local flow viscosity.

2.3 Fundamentals of Rayleigh light scattering (RLS) in a propane–(air–neon) mixture

Rayleigh light scattering is used for monitoring concentration fluctuations. It has been proved that it is an excellent technique for performing quantitative time-space-resolved measurements in a multi-components turbulent flow (Pitts and Kashiwagi 1984). The total Rayleigh scattered light intensity in the perpendicular direction to the light source, noted $I(90^\circ)$, depends on the known incident intensity I_o passing through an ideal gas with j components in the following way (Zhao and Hiroyasu 1993):

$$I(90^\circ) = CNI_o \sum [\chi_i \sigma_i], \quad (11)$$

where

$$\sum \chi_i = 1, \quad (12)$$

where C is a system calibration constant that accounts for the optical collection and transmission efficiencies; $N = PA_o/RT$, ($\sum N_i = N$) is the total number of molecules contained in the probe volume, P and T are, respectively, the standard

pressure and the temperature, and A_o is the Avogadro number, and R is the universal gases constant. Finally, σ_i is the differential Rayleigh cross section without molecular anisotropy effects (depolarization), defined as follows:

$$\sigma_i = 4\pi^2 [n_i - 1]^2 / [\lambda w^4 N_o^2], \quad (13)$$

where n_i is the index of refraction of the gas at standard temperature and pressure, λw is the laser wavelength (here equal to 676 nm) and N_o is the Loschmidt number ($2.687 \times 10^{19} \text{ cm}^{-3}$). For a ternary isothermal mixture composed of propane, neon and air, Eq. 11 can be transformed to:

$$I(90^\circ) = [\sigma_{air} \chi_{air} + \sigma_{neon} \chi_{neon} + \sigma_{propane} \chi_{propane}] CNI_o, \quad (14)$$

where σ_{air} , σ_{neon} and $\sigma_{propane}$ are the observed 90° scattering cross sections for pure air, pure neon and pure propane, respectively. For the 676 nm laser wavelength, the respective theoretical values of the cross sections are $5.3 \times 10^{-27} \text{ cm}^{-2}$ (Sutton and Driscoll 2004), $0.25 \times 10^{-27} \text{ cm}^{-2}$ (Shardanand and Prasad Rao 1977) and $72 \times 10^{-27} \text{ cm}^{-2}$ (Sutton and Driscoll 2004).

Assuming that pressure, temperature and laser intensity are constant, the molar-conservation equation, viz. Eq. 12, can be written as

$$\chi_{air} + \chi_{neon} + \chi_{propane} = 1. \quad (15)$$

Strictly mathematically speaking, the system composed of Eq. 14 and 15 cannot be directly solved. By noting that the molecular diffusion coefficients of propane into air and of propane into neon are four times weaker than those of air into neon ($D_{air-C_3H_8} \approx 9.09 \times 10^{-6}$, $D_{neon-C_3H_8} \approx 8.24 \times 10^{-6}$ and $D_{air-neon} \approx 3.42 \times 10^{-5} \text{ m}^2 \text{ s}^{-1}$) and by noting that air and neon are mixed in the co-flow before they meet propane, we conclude that the mass fraction of

neon present in a blob of oxidizer ('air–neon') remains nearly constant when this particle is mixed with propane into the turbulent flow, at the first order. Moreover, the very small ratio $\sigma_{\text{neon}}/\sigma_{\text{propane}} = 1/288$ and $\sigma_{\text{air}}/\sigma_{\text{propane}} = 1/21$ insures very small contribution of neon in Eq. 14 and, therefore, in estimating propane mass fraction with RLS. This is a particular advantage of using neon for RLS measurement. Therefore, the mixture we investigate here will be further considered as a binary one and will be noted as propane–(air–neon). The molecular diffusion coefficient of this binary mixture will be noted as $D_{\text{C}_3\text{H}_8\text{--oxidizer}}$. In conclusion, the initial system of 2 equations with 3 unknowns becomes now with only 2 unknowns, therefore solvable, because neon is practically invisible from the Rayleigh light-scattering viewpoint. We remind here that the neon is obviously very present from a thermal viewpoint and modifies the heat exchanged at the level of the hot wire.

Therefore, a constant equivalent Rayleigh cross section can be defined for the oxidizer as $\sigma_{\text{mix}} = \sigma_{\text{air}} [1 - \chi_{\text{opt}}] + \sigma_{\text{neon}}\chi_{\text{opt}} = 1.94 \times 10^{-27} \text{ cm}^{-2}$, where $\chi_{\text{opt}} = 0.70$ is the molar fraction of neon optimized for independent measurement of velocity in propane–air–neon mixture. This assumption allows us writing the following equivalent system for RLS when neon is added:

$$I(90^\circ) = [\sigma_{\text{mix}}(1 - \chi_{\text{propane}}) + \sigma_{\text{propane}}\chi_{\text{propane}}]CNI_o, \quad (16)$$

that leads to a solvable system. The molar fraction of propane is thus deduced from this system of equations as:

$$\chi_{\text{propane}} = [I - I_{\text{air--neon}}]/[I_{\text{propane}} - I_{\text{air--neon}}], \quad (17)$$

where the index '(90°)' has been dropped off for sake of simplicity. Relation 17 allows for obtaining the molar fraction of propane, and hence the mass fraction of the propane, hereafter denoted Y ($1 - Y$ denotes the mass fraction of air–neon).

The hot wire positioned in the vicinity of the Rayleigh probe volume does not perturb the Rayleigh signal by light reflections. Indeed, the measured Rayleigh cross sections ratios $\sigma_{\text{propane}}/\sigma_{\text{air}}$ and $\sigma_{\text{propane}}/\sigma_{70\%\text{neon}+30\%\text{air}}$ are in agreement with the theoretical values (13.6 ± 0.1 and 50.8 ± 0.3 respectively). These values are found for twenty different data sets recorded during the same day. Excellent agreement between the measured and the predicted values is obtained (the difference is smaller than 0.7%). Note that adding neon provides much more SNR (Signal to Noise Ratio) for the Rayleigh light scattering. This is another interesting advantage of using neon for RLS measurement.

3 Experimental setup and measurements conditions

The flow system consists of an axisymmetric jet of propane issuing into a slow co-flow of air (Fig. 4). The jet and the

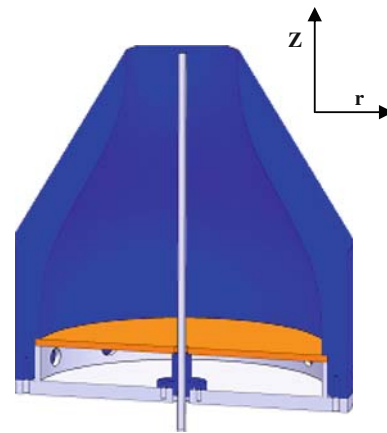


Fig. 4 Axisymmetric jet with co-flow

co-flow diameters are $D = 5 \text{ mm}$ and $D_{\text{co-flow}} = 80 \text{ mm}$, respectively. The internal convergent is profiled such that reverse flows are absent. Elements for flow laminarization are disposed in the annular co-flow ring. Because Rayleigh light-scattering measurements are extremely sensitive to the interference with particle scattering (Mie), particular attention has been paid to eliminate dust particles that might be present in the flows (of either air or propane). The co-flow velocity is fixed to 0.1 m s^{-1} , which is sufficient to remove particles without altering the mixing jet properties. The jet is mounted on a 2D displacement system Charly-Robot with $10 \mu\text{m}$ precision in position. Flows of both propane and air–neon are controlled and measured with Bronkhorst® digital flowmeters. The accuracy of the flow rate is better than 0.3%.

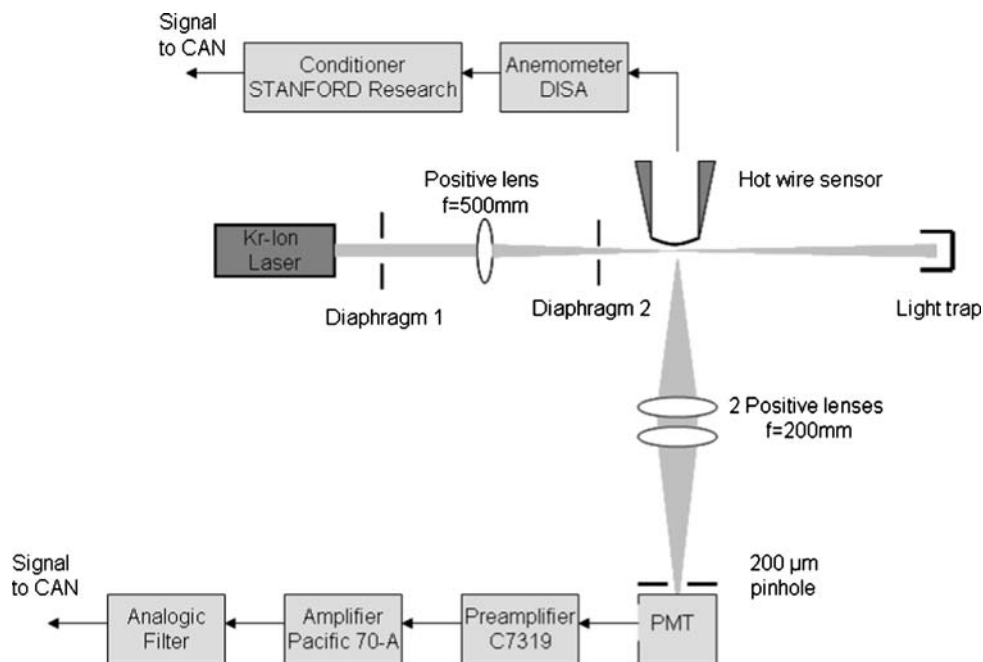
In this study, two different flow conditions are tested:

- a propane jet discharging into a stagnant 30% air–70% neon mixture (as discussed in the previous section) with an initial Reynolds number $Re_D = U_0 D/\nu = 15400$, where U_0 is the jet nozzle velocity, and ν is the kinematic viscosity of the internal jet and with an initial momentum flux per unit area $M_0 = \rho_0 U_0^2$ of $360 \text{ kg m}^{-1} \text{ s}^{-2}$, where ρ_0 is the density of the internal jet fluid;
- an air jet discharging into stagnant air at the same initial jet momentum per unit area, $M_0 = 360 \text{ kg m}^{-1} \text{ s}^{-2}$, and for which $Re = 5400$.

A sketch of the coupling RLS and HWA experimental setup is shown on Fig. 5.

A Spectra-Physics Model 171–01 Krypton-ion laser is operated to produce a 6 W output in the single wavelength of 676 nm. The intensity profile of the laser-beam waist is gaussian at the exit of the laser, with a mean diameter of about 1.9 mm. It is focused by a positive lens of focal length = 500 mm to a narrow cylinder of 80 μm diameter (checked with a camera). The Rayleigh measurement

Fig. 5 Schematic of the RLS and HWA measurement systems



volume is about 5 mm long. Two diaphragms 1 and 2 in Fig. 5 are positioned along the laser beam to limit the light diffraction phenomena coming from lens and laser beam. Light scattered from the observation volume is collected and collimated by an anti-reflection coating 200 mm lens ($f/2$) and then refocused by another identical lens toward the Photo Multiplier Tube (PMT). A 200 μm pinhole is placed between the second lens and the PMT to limit the axial dimension of the Rayleigh probe volume. No band-pass filter is used for a maximum of light scattered intensity on the photocathode of the PMT. The scattered light is collected by a Hamamatsu PMT model H6780-20 with a selected photocathode of 0.15 nA low dark current. The output signal of the PMT is then amplified by a preamplifier Hamamatsu C7319 tuned to a calibrated gain of 10^6 and by an analogical amplifier PACIFIC 70-A.

The Rayleigh signal coming from the PMT is first cleaned from residual Mie scattering particles with a specific data analysis algorithm in order to select only the samples free of these undesirable effects. Dark noise is considerably reduced by our selected photocathode PMT (dark current less than 0.15 nA). Uncertainties induced by shot noise are evaluated both theoretically and experimentally, using the methods presented by (Gustavsson and Segal 2005; Pitts and Kashiwagi 1984; Pollock 1994).

Table 3 summarizes the arrival rate measured by the PMT and estimated experimentally R_p^{exp} , the arrival rate calculated analytically R_p^{theo} , and the relative uncertainty due to electronic shot noise for the experimental case. The results are given for measurements in pure propane and in pure air, for the following operating conditions: a laser output of 5.7 W (i.e. 2.9×10^{-19} photons s^{-1}), the optical system described previously and a room temperature of 296 K. Theoretical results agree well with the corresponding measured data. As expected, the contributions of electronic shot noise are maximum for the lower concentrations (i.e. for the lowest intensity of light scattered) but do not exceed 3%.

For the velocity measurements, a Pt/Rh 90/10% hot wire with a length $l = 400 \mu\text{m}$ and $d = 2.5 \mu\text{m}$ diameter is used. This insures a ratio $l/d = 160$ (the optimal ratio ~ 200). The hot-wire probe is driven in constant temperature mode by a DISA 55M01 anemometer. Voltage fluctuations are then amplified using a built-on signal conditioner in order to improve signal to noise ratio. The physical cut-off frequency for the hot wire has been measured at 40 kHz with a calibrated square signal, which is beyond the Kolmogorov frequency in our flow conditions.

The signals (RLS and HWA) are low-pass filtered by an analog filter SRS 983 at 35 kHz and 50 kHz, respectively.

Table 3 Uncertainties on Rayleigh light-scattering measurements due to the shot noise

	R_p^{theo}	R_p^{exp}	$\Delta_{R_p, \Delta t}$ (at $F_s = 100$ kHz)
Pure propane	2.55×10^9 photons s^{-1}	1.9×10^9 photons s^{-1}	0.7%
Pure air	1.9×10^8 photons s^{-1}	1.3×10^8 photons s^{-1}	2.8%

We also checked that the cut-off frequencies of the RLS measurement system are situated beyond these filtering frequencies (35 kHz) of the Rayleigh light scattering and of the hot-wire anemometry (50 kHz). After conditioning, both signals are sent to a 16 bits National Instrument NI-9215 acquisition card. For each flow condition, at least 130,000 integral time scales are acquired.

In order to reduce the spatial-filtering effects on the velocity measurement, the length of the hot-wire probe was reduced as much as possible (400 μm for the sensitive length of the hot-wire probe), close to the optimal ratio ~200 and representing between 3 and 8 Kolmogorov scales in the propane and 2.5–5 Kolmogorov scales in the pure air jet.

Spatial-filtering corrections with, e.g., Pao model of spectrum (Pao 1965) are applied. These are in full agreement with the correction method proposed by (Lavoie et al. 2007), for one-point measurements. However, the full strength of the method discussed in Lavoie et al. (2007) resides in a correct accounting for the 2D spatial filtering (most useful in the case of PIV measurements), which is not relevant in the case of the one-point measurements we use here. No correction was used for the Rayleigh measurements. Indeed, the Rayleigh probe volume of 200 μm is close to the Batchelor scale, which is of about 50 μm at $Z/D = 4$ and 200 μm at $Z/D = 30$.

4 Validation of the new HWA technique and of the concentration measurement

In this section, some results obtained with our new HWA technique as well as with the RLS are critically compared

with classical results. The downstream axial evolution of the mean velocity and concentration fields are first presented in Sect. 4.1, then the radial profiles of the mean and RMS quantities (velocity and scalar) are discussed in Sect. 4.2. The results obtained agree very well with the literature of variable density/viscosity jets.

4.1 Downstream evolution of the mean velocity and concentration along the jet axis

The mean axial velocity, on the jet axis, is noted as $\langle U_c \rangle$ (the subscript c refers to the jet axis centerline). The axial evolution of the inverse of $\langle U_c \rangle$ is plotted in Fig. 6 (left) for a propane jet discharging into air–neon mixture and for an air jet discharging into stagnant air, at $M_0 = 360 \text{ kg m}^{-1} \text{ s}^{-2}$. Two different representations are illustrated:

1. The first one is a representation of $U_0/\langle U_c \rangle$ as a function of Z/D (the subscript 0 refers to the initial conditions). This representation does not take into account the fluids densities. It shows that this evolution is hyperbolic but not universal.
2. A second one in which density effects, although small ($\rho_{C_3H_8}/\rho_{\text{air-neon}} = 1.52$), are taken into account. A test of the longitudinal pseudo-similarity (Chen and Rodi 1980) is pertinent in the pure jet region where forces of inertia dominate. This pure jet region extends as far as the dimensionless abscissa $Z_b = Fr^{-1/2}(\rho_{\text{propane}}/\rho_{\text{air-neon}})^{-1/4}$ (Z/D) is smaller than 0.53, where the Froude number $Fr = \rho_{\text{propane}}U_0^2/gD|\rho_{\text{air-neon}} - \rho_{\text{propane}}|$, g is the local gravity ($9.81 \text{ m}^2 \text{ s}^{-1}$). For the test conditions presented in Table 4, $Fr = 7400$, and, therefore, Z_b varies from 0.04 to 0.31 from $Z/D = 4$ to $Z/D = 30$, satisfying the hypothesis of pure jet region for all the

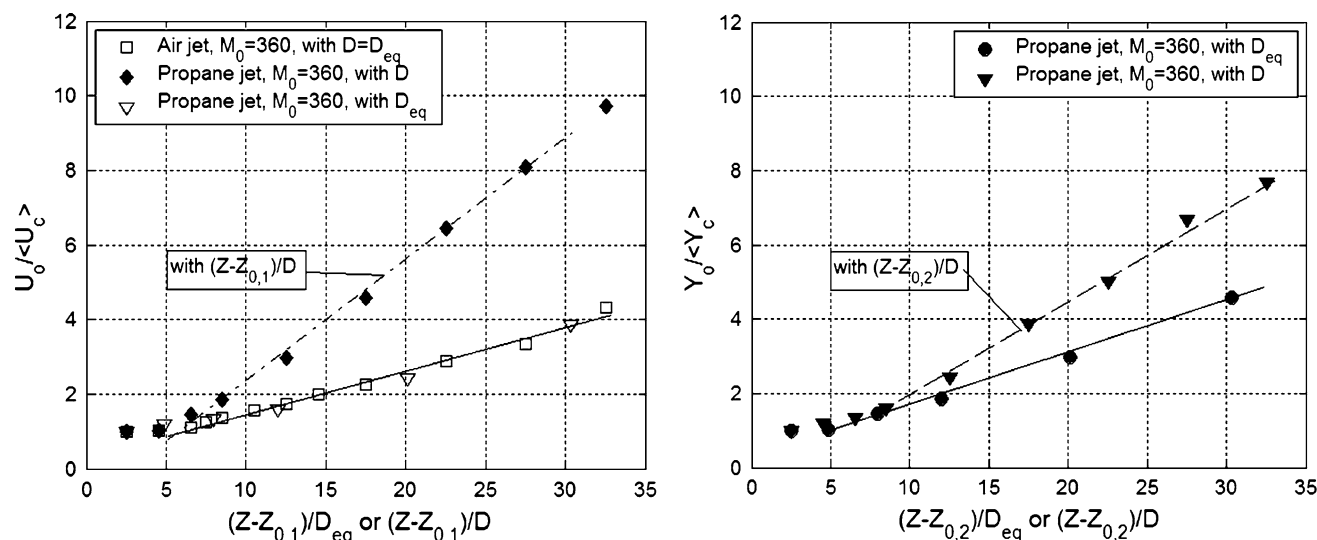


Fig. 6 Test of pseudo-similarity for the velocity (left) and for the scalar (right) as suggested by (Chen and Rodi 1980)

Table 4 Characteristics of the propane jet ($Re_D = 15400$, $M_o = \rho_{\text{propane}} U_{\text{propane}}^2 = 360$) and air jet ($Re_D = 5400$, $M_o = \rho_{\text{air}} U_{\text{air}}^2 = 360$) at centerline locations from $Z/D = 4$ –30

Z/D	$\langle U_c \rangle$ (m s ⁻¹)	$\langle u_c^2 \rangle^{1/2}$ (m s ⁻¹)	T_I (μ s)	L_I (mm)	λ_T (μ m)	Re_λ	λ_K (μ m)	$\langle \varepsilon \rangle_{\text{iso}}$ (m ² s ⁻³)	$\langle Y_c \rangle$	$\langle y_{ic}^2 \rangle^{1/2}$	$\langle v_c \rangle$ (m ² s ⁻¹) $\times 10^{-5}$
0											
Propane jet (in air–neon)	14.2								1.00		0.463
Air jet (in air)	17.3										
4											
Propane jet (in air–neon)	9.70	0.72	113	1.1	552	42	43	237	0.75	0.068	0.941
Air jet (in air)	16.4	0.85	248	4.0	343	18	82	90			
6											
Propane jet (in air–neon)	7.55	1.35	174	1.3	488	60	32	1280	0.63	0.107	1.103
Air jet (in air)	14.7	1.12	302	5.2	390	24	74	135			
10											
Propane jet (in air–neon)	4.70	1.12	319	1.5	510	16	39	1722	0.41	0.105	1.596
Air jet (in air)	10.5	1.25	590	5.7	697	54	86	73			
15											
Propane jet (in air–neon)	3.05	0.72	560	1.7	548	14	62	410	0.26	0.091	1.832
Air jet (in air)	8.0	1.16	1026	8.1	845	60	108	31			
20											
Propane jet (in air–neon)	2.17	0.51	890	1.8	861	17	104	70	0.20	0.071	2.026
Air jet (in air)	6.70	1.05	1433	9.7	912	60	126	17			
25											
Propane jet (in air–neon)	1.73	0.40	1130	2.0	970	15	128	37	0.15	0.057	2.157
Air jet (in air)	5.90	0.90	2095	11.9	1127	60	149	8.5			
30											
Propane jet (in air–neon)	1.44	0.33	1700	2.3	1200	15	154	19	0.13	0.047	2.211
Air jet (in air)	5.0	0.85	3012	15.1	1402	60	181	4.0			

conditions explored. The equivalent diameter $D_{\text{eq}} = D [\rho_j / \rho_{\text{air–neon}}]^{1/2}$ is hence used for collapsing the data (Graham et al. 1974). Here, ρ_j refers to the local density along the jet axis. When these effects are taken into account (via a representation of $U_o / \langle U_c \rangle$ as a function of Z/D_{eq}), the collapse of the inverse of the axial velocity is almost perfect and in full agreement with those obtained by (Amielh et al. 1996) and (Chen and Rodi 1980) for CO₂/air jet (for which $\rho_{\text{CO}_2} / \rho_{\text{air}} \approx 1.50$), and also for pure air and helium jets. A shift of the origin is here necessary by considering the virtual origin of the velocity field, $Z_{0,1}$. These results confirm that the hyperbolic decreasing in axial variations of the longitudinal velocity is independent of the initial density ratio for gases discharging into an environment with similar or different viscosity (Thring and Newby 1952).

The axial evolution of the mean concentration, $\langle Y_c \rangle$, is plotted in Fig. 6 (right). As for the velocity, the mean axial concentration follows a hyperbolic decreasing law, which is universal when plotted via a representation of $Y_o / \langle Y_c \rangle$ as a function of Z/D_{eq} . Furthermore, we note that the concentration decays faster than the mean velocity. This

observation is consistent with the following statement: “the scalar mixes better than the momentum” as mentioned in, e.g., (Lubbers et al. 2001). An extrapolation of the axial evolution until $Y_o / \langle Y_c \rangle = 1$ gives $\langle Y_c \rangle = 1$ at $Z/D = 2$. In order to determine the slopes of the curves on Fig. 6, the data have been fitted by a least-mean-squares algorithm to the following equations:

$$\frac{\langle U_c \rangle}{U_o} = k_u \left[\frac{D_{\text{eq}}}{Z - Z_{0,1}} \right]; \quad (18)$$

$$\frac{\langle Y_c \rangle}{Y_o} = k_Y \left[\frac{D_{\text{eq}}}{Z - Z_{0,2}} \right]. \quad (19)$$

The virtual origins $Z_{0,1}/D$ for velocity and $Z_{0,2}/D$ for concentration found for the propane jet are, respectively, -2.52 and -0.85 , which are also consistent with results already reported for propane jets (Dibble et al. 1987; Dowling and Dimotakis 1990) and in excellent agreement with the value $Z_{0,1}/D = -2.9$ reported for CO₂/air jet in similar conditions (Amielh et al. 1996). We find $k_u = 6.2$ and $k_Y = 5.3$. These values are very close to the values of 6.1 and 5.5, respectively, reported in (Lubbers et al. 2001). The concentration evolution is similar to those for a CO₂

jet and air jet with a dye (Djeridane et al. 1996) and in excellent agreement with those reported in (Pitts and Kashiwagi 1984) for a methane round jet.

In Fig. 7, the value of $k_Y = (Z - Z_{0,2}) \langle Y_c \rangle / [Y_0 D]$ is shown versus the distance to the jet orifice is shown (here, D is used instead of D_{eq}). Also plotted in this figure are the experimental values obtained by (Becker et al. 1967; Birch et al. 1978; Dowling and Dimotakis 1990; Lockwood and Moneib 1980) and DNS results by (Lubbers et al. 2001). The factor k_Y varies between 4 and 6, in very good agreement with literature data.

As a conclusion, the variations of either $\langle U_c \rangle$ or $\langle Y_c \rangle$ are hyperbolic for both of them when represented as functions of Z/D . By taking into account the (here, slight) density variations through a representation as functions of Z/D_{eq} , these evolutions are both hyperbolic and universal.

4.2 Radial profiles of mean and RMS values of velocity and concentration

Let us now turn our attention to the radial profiles of velocity and scalar fields.

Following (Amielh et al. 1996; Ruffin et al. 1994), density effects do not seriously affect the radial expansion of the jet, contrary to the axial decay of the mean velocity, which is affected by the local density. This is most likely due to the similar radial evolution for both velocity and concentration, thus hiding the density effects. Therefore, the real diameter D (and not the equivalent diameter D_{eq}) governs the radial spreading of variable density jets.

Figure 8 shows the radial profiles of the mean and root-mean-square of both velocity ($\langle U \rangle$ and $\langle u^2 \rangle^{1/2}$, respectively) and scalar ($\langle Y \rangle$ and $\langle y^2 \rangle^{1/2}$, respectively)

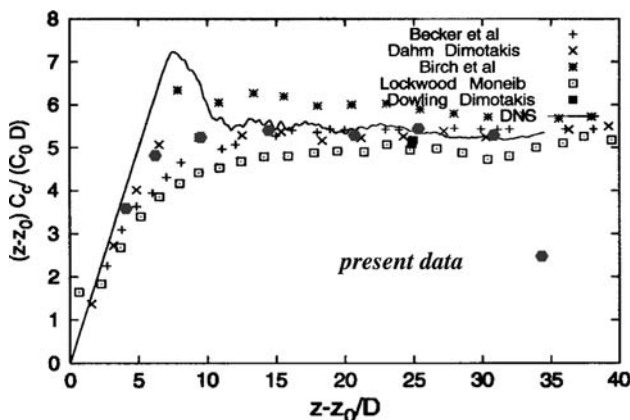


Fig. 7 Present data $k_Y = (Z - Z_{0,2}) Y_c / (Y_0 D)$ versus the distance to the virtual origin $(Z - Z_{0,2})/D$ (filled circles) compared to the data from Lubbers et al. (2001), Lockwood and Moneib (1980), Dahm and Dimotakis (1987), Becker et al. (1967), Dowling and Dimotakis (1990) and Birch et al. (1978). From Lubbers et al. (2001). Note here the conversion $C_c \rightarrow Y_c$, $C_o \rightarrow Y_o$ and $z_o \rightarrow Z_{0,2}$ to the notations used in this paper

versus the non-dimensional coordinate $\eta_i = r/(Z - Z_{0,i})$ (with $i = 1$ for velocity, $i = 2$ for the mixture fraction or concentration), with no consideration of the equivalent diameter. Mean and RMS quantities are normalized by the mean values on the jet axis, $\langle U_c \rangle$ and $\langle Y_c \rangle$ for $Z/D = 4, 6$ and 15 .

All the mean quantities from $Z/D = 4$ – 15 collapse on a unique curve (solid line on Fig. 8, left) that could be fitted by the following expressions, for the velocity and for the concentration, respectively:

$$\frac{\langle U \rangle}{\langle U_c \rangle} = \exp[-K_u \eta^2]; \quad (20)$$

$$\frac{\langle Y \rangle}{\langle Y_c \rangle} = \exp[-K_Y \eta^2], \quad (21)$$

with $K_u = 77.4$ and $K_Y = 58.2$. The velocity profiles agree well with the self-similar profiles obtained for an air jet by either DNS at $Re_D = 2400$ ($K_u = 76.1$) (Boersma et al. 1998), or experimentally at $Re_D = 11000$ ($K_u = 75.2$) (Panchapakesan and Lumley 1993). Because density effects are not visible for this representation, the present results are also in excellent agreement with those from variable density jets (CO_2 at $Re_D = 32000$ and He at $Re_D = 4000$) as reported by (Amielh et al. 1996). The concentration profile is close to those obtained by the DNS of (Lubbers et al. 2001) at $Re_D = 2000$ ($K_Y = 59.1$). Note that the difference between the coefficients K_u and K_Y ($K_u > K_Y$) has the significance of a better scalar radial mixing compared to the momentum radial diffusion. In addition, normalized mean profiles for both velocity and scalar reach rapidly self-similarity (obtained at $Z/D = 4$ only) compared with classical results for constant-viscosity jets, for which self-similarity for the two-first moments is not obtained before $Z/D = 15$. This is most likely due to:

1. the large viscosity variations between propane ($\nu_{\text{propane}} \sim 4.63 \times 10^{-6} \text{ m}^2 \text{ s}^{-1}$) and quiescent air–neon mixture ($\nu_{\text{air–neon}} \sim 24.99 \times 10^{-6} \text{ m}^2 \text{ s}^{-1}$, $\nu_{\text{air–neon}}/\nu_{\text{propane}} = 5.5$) that accelerate the momentum diffusion at a more intense level than in a constant-viscosity flows. Although of smaller importance, large viscosity gradients would also be present for a propane jet discharging in stagnant air ($\nu_{\text{air}} \sim 16.04 \times 10^{-6} \text{ m}^2 \text{ s}^{-1}$, $\nu_{\text{air}}/\nu_{\text{propane}} = 3.4$),
2. the high ratio between the thickness of the injection nozzle and the diameter of the jet (equal to $1/10$) that leads to a large-width initial shear layer between propane and pure oxidizer, which in turn results in initially created large vortical structures, thus accelerating mixing and the jet development.

RMS profiles of the velocity and concentration are presented on Fig. 8 (right) for the same downstream

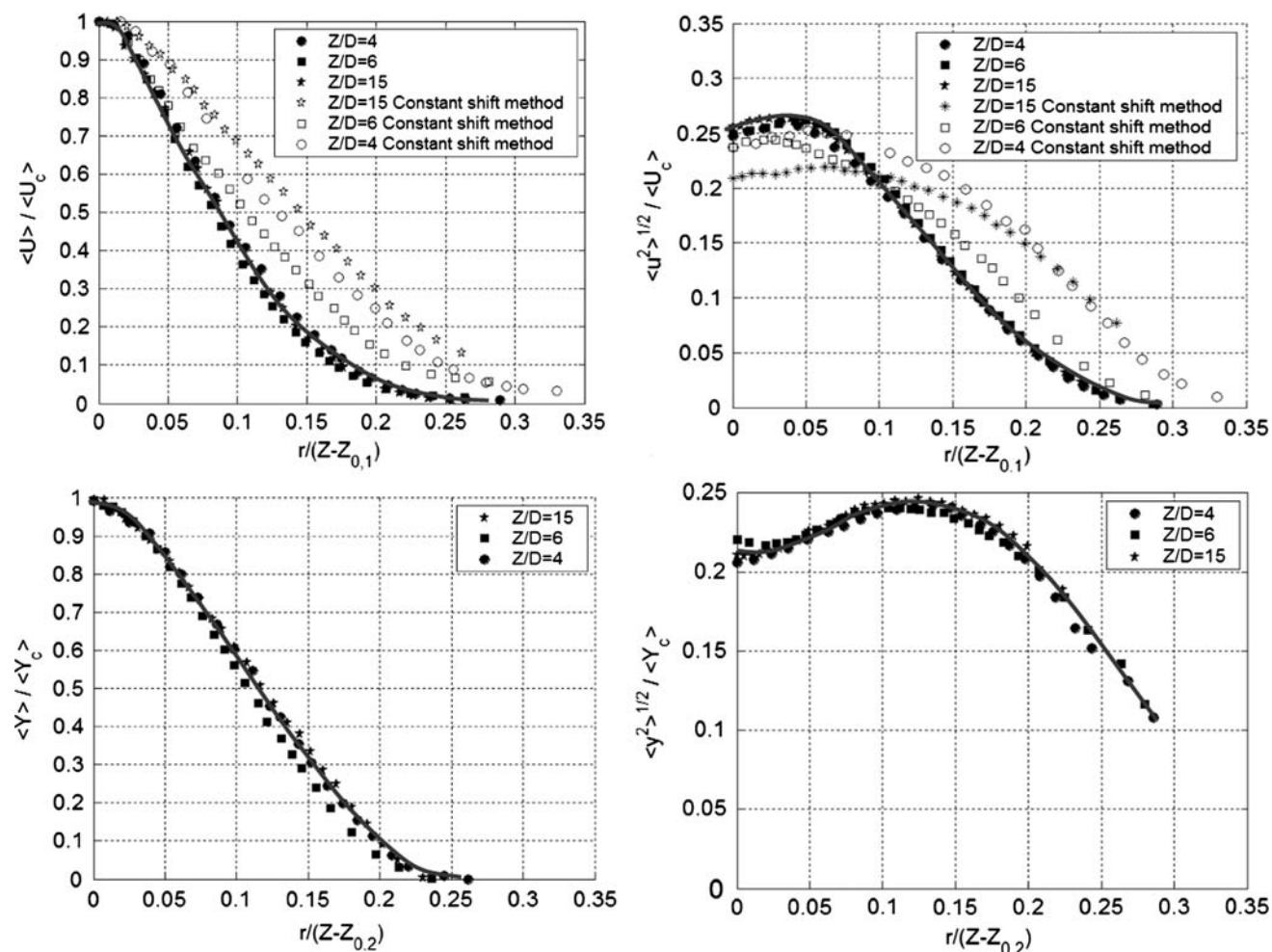


Fig. 8 Mean and RMS values of velocity (*top*) and concentration (*bottom*) at different axial locations: $Z/D = 4, 6$ and 15 , for propane jet with $Mo = 360$ discharging into 30% air–70% neon

positions ranging from 4 to 15 diameters. The normalized peak magnitudes of fluctuating quantities (0.26 and 0.25 for velocity and scalar, respectively, at $\eta = 0.05$ and $\eta = 0.11$) are consistent with already published results for velocity and scalar in a propane jet (Lubbers et al. 2001; Papanicolaou and List 1988; Schefer and Dibble 1986), or heavy jets (Chassaing et al. 1994; Richardson and Pitts 1993). All the data collapse and the corresponding least-squares fits (solid lines) are shown. For the concentration, the solid line represents a fourth-order polynomial fit:

$$\frac{\langle Y \rangle}{\langle Y_c \rangle} = A\eta [a_1 + a_2\eta + a_3\eta^2 + a_4\eta^3 + a_5\eta^4], \quad (22)$$

where $A = 9.34$; $a_1 = 0.18$; $a_2 = 0.41$; $a_3 = 8.88$; $a_4 = -117.6$; $a_5 = 251.6$. These values are very close to the fit found by (Richardson and Pitts 1993).

The radial profiles of mean and RMS of velocity obtained with the ‘Constant-shift’ method presented in Sect. 2.1 are also plotted. Self-similarity is not respected, and the profiles are inconsistent with literature data. We

thus emphasize that this method is not consistent with physical results, and thus underline the utility of the new method for measuring the fluctuating velocity field, which is described in this material.

At this stage, the HWA and RLS techniques have been validated, because all the mean/RMS profiles agree very well with published data on jets. Moreover, for low-order statistics (mean and RMS values), we note no major difference between our variable-viscosity jet and constant-viscosity jets (described in the literature).

5 Turbulent properties along the axis of a propane jet discharging into 30% air–70% neon ($v_{\text{air-neon}}/v_{\text{propane}} = 5.5$) and an air jet ($v = \text{constant}$) at the same initial jet momentum

In this section, we make use of HWA and RLS measurements in order to provide a deeper characterization of a jet flow with moderate viscosity effects ($v_{\text{air-neon}}/v_{\text{C}_3\text{H}_8} = 5.5$).

Turbulent properties along the axis of a propane jet ($Mo = 360 \text{ kg m}^{-1} \text{ s}^{-2}$) discharging into a stagnant 30% air–70% neon mixture, and having moderate viscosity gradients (up to 5.5) are analyzed. The turbulent kinetic energy, three (isotropic) forms of the mean energy dissipation rate, turbulent length scales and the Reynolds number based on the Taylor microscale are compared to the corresponding quantities in an air jet at the same initial momentum flux per unit area, $Mo = 360 \text{ kg m}^{-1} \text{ s}^{-2}$. The analysis is performed along the jet axis (the results out of the axis will be reported elsewhere). Differences observed are discussed and viscosity effects are highlighted. Finally, both velocity and scalar spectra are analyzed.

5.1 Characterization of turbulence along the jet axis

The variations of turbulent intensities $\langle u^2 \rangle^{1/2} / \langle U_c \rangle$ along the axis of the jet of propane and air are plotted in Fig. 9, left. For the air jet, self-similarity (for which turbulent intensity is to be constant) seems to be reached since $Z/D = 12$. A very rapid (linear) increase in the axial turbulent intensity up to $Z/D = 12$ and a very slow increase beyond this position are observed.

On the contrary, self-similarity for the propane jet discharging into air–neon mixture is likely to be achieved at a much earlier downstream location ($Z/D = 8$) than for the air jet. Moreover, the maximum magnitude is higher than that for the air jet, and only a slight decrease is noted at the beginning of the “far-field” region. This intensification of turbulence in the propane jet is due to strong viscosity gradients, associating fluid blobs originating from propane, with fluid blobs coming from the ambient air–neon, much more viscous.

The axial turbulent intensities of concentration are presented on Fig. 9 right side. Axial intensities of the concentration fluctuations $\langle y^2 \rangle^{1/2} / \langle Y_c \rangle$ increase linearly up to $Z/D \sim 15$ before remaining at the constant value 0.37. Figure (9) shows that, as far as the propane jet is concerned, the boundary between “near-field” and “far-field” for the velocity (at $Z/D = 8$) differs from that of the concentration (at $Z/D \sim 15$). The ‘delay’ in attaining the self-similar state by the concentration field is most likely due to the increasing Schmidt number for increasing downstream positions, later discussed in Sect. 5.2. This increasing Schmidt number is associated with smaller and smaller (in comparison to the Kolmogorov scale) scales to be created by mixing.

Before characterizing the different scales of the flow (integral, Taylor, Kolmogorov), it is essential to first characterize the mean energy dissipation rate, $\langle \varepsilon \rangle$, for which the full expression in constant-viscosity turbulence is given by (Sreenivasan 1984):

$$\langle \varepsilon \rangle = \frac{\nu}{2} \left\langle \left(\frac{\partial u_i}{\partial x_j} + \frac{\partial u_j}{\partial x_i} \right)^2 \right\rangle, \tag{23}$$

where double indices indicate summation. We insist on the fact that Eq. 23 only holds in constant-viscosity fluids. In variable-viscosity flows, it provides only an approximation of the true mean energy dissipation, when it takes into account the mean value of the local kinematic viscosity. Even under these simplified conditions, the experimental estimation of all the terms in the right-hand-side of Eq. 23 is known to be very difficult. With only one component measured, the simplest estimate of the mean energy dissipation rate, standing on local isotropy assumption, is given by

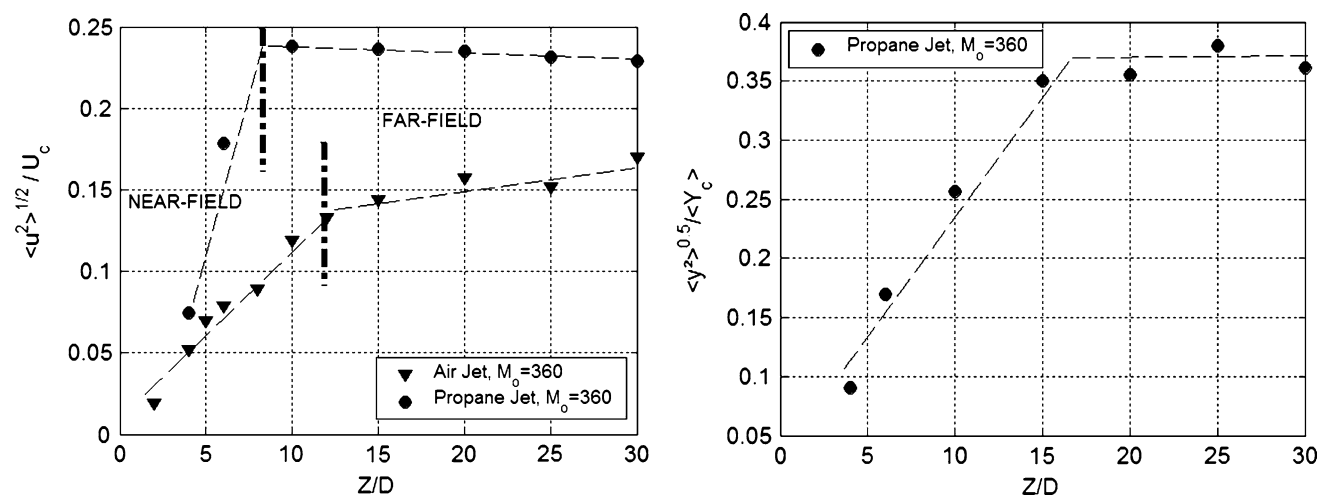


Fig. 9 Variation of turbulent intensities along the jet axis, for the velocity field (left) and propane concentration (right)

$$\langle \varepsilon \rangle_{iso}^1 = 15 \langle v_c \rangle \left\langle \left(\frac{\partial u}{\partial Z} \right)^2 \right\rangle, \quad (24)$$

where $\langle v_c \rangle$ is the local mean kinematic viscosity at the jet axis location (determined from the mass fraction $\langle Y_c \rangle$) considered, and superscript ‘1’ indicates that this is the first method we use here. By further assuming the validity of Taylor’s hypothesis, Eq. 24 becomes:

$$\langle \varepsilon \rangle_{iso}^1 = 15 \frac{\langle v_c \rangle}{\langle U_c \rangle^2} \left\langle \left(\frac{\partial u}{\partial t} \right)^2 \right\rangle. \quad (25)$$

Furthermore, if $E_{11}(k_1)$ is the spectral density of the longitudinal velocity fluctuations, where the wavenumber k_1 is related to frequency f , we can write the equivalent equation (“method 2”)

$$\langle \varepsilon \rangle_{iso}^2 = 15 \langle v_c \rangle \int_0^{+\infty} k_1^2 E_{11}(k_1) dk_1, \quad (26)$$

or, equivalently:

$$\langle \varepsilon \rangle_{iso}^2 = 15 \left(\frac{2\pi}{\langle U_c \rangle} \right)^2 \langle v_c \rangle \int_0^{+\infty} f^2 E_{11}(f) df. \quad (27)$$

Equations 25 and 27 are two commonly used methods for estimating the mean value of $\langle \varepsilon \rangle$. Both of them hold for locally isotropic turbulence. They are strictly equivalent under the condition that the 1D spectrum covers the whole range of scales down to Kolmogorov. These two expressions are calculated for both propane and air jets. The results are plotted on Fig. 10, showing an excellent agreement among them, thus meaning that the velocity spectra are well resolved. For the propane jet, the local

viscosity $\langle v_c \rangle$ at the hot-wire location is estimated from the mean concentration measurement at an upstream location of 800 μm . The values of $\langle v_c \rangle$ are computed by using the kinetic theory of non-uniform gases (Hirschfelder et al. 1966). For different axial locations $Z/D = 4, 6, 10, 15, 20, 25$ and 30 , they are equal to $9.41 \times 10^{-6} \text{ m}^2 \text{ s}^{-1}$, $1.103 \times 10^{-5} \text{ m}^2 \text{ s}^{-1}$, $1.596 \times 10^{-5} \text{ m}^2 \text{ s}^{-1}$, $1.832 \times 10^{-5} \text{ m}^2 \text{ s}^{-1}$, $2.026 \times 10^{-5} \text{ m}^2 \text{ s}^{-1}$, $2.157 \times 10^{-5} \text{ m}^2 \text{ s}^{-1}$, $2.211 \times 10^{-5} \text{ m}^2 \text{ s}^{-1}$, respectively. The viscosity in the air jet is taken constant at $16.03 \times 10^{-6} \text{ m}^2 \text{ s}^{-1}$.

A third method to infer the mean energy dissipation rate stems in using the 1-point energy budget equation. It is obtained from Navier–Stokes equations written for each velocity component by multiplying each of them by the fluctuating velocity itself, averaging and summing the three transport equations. For the jet axis, the energy dissipation rate is only balanced by two terms: the kinetic energy decay along the jet axis and the production term (proportional to the decay of the mean velocity along the jet axis and with the difference between the variance of radial velocity fluctuations and the variance of the axial velocity fluctuations $\langle v^2 \rangle - \langle u^2 \rangle$). We do not dispose on $\langle v^2 \rangle$, but it is reasonable to assume that strong viscosity gradients present in this flow lead to rapid mixing and therefore to a better isotropy (Lee et al. 2008), which leads in turn to negligible differences among variances of the two velocity components, so to a negligible production term. Therefore, with the assumption that the production term of turbulent energy is small enough (along the jet axis), the mean energy dissipation rate can be written under the same form as that used in decaying grid turbulence:

$$\langle \varepsilon \rangle_{iso}^3 = -\frac{\langle U_c \rangle d\langle q^2 \rangle}{2 dZ} = -\frac{3\langle U_c \rangle d\langle u^2 \rangle}{2 dZ} \quad (28)$$

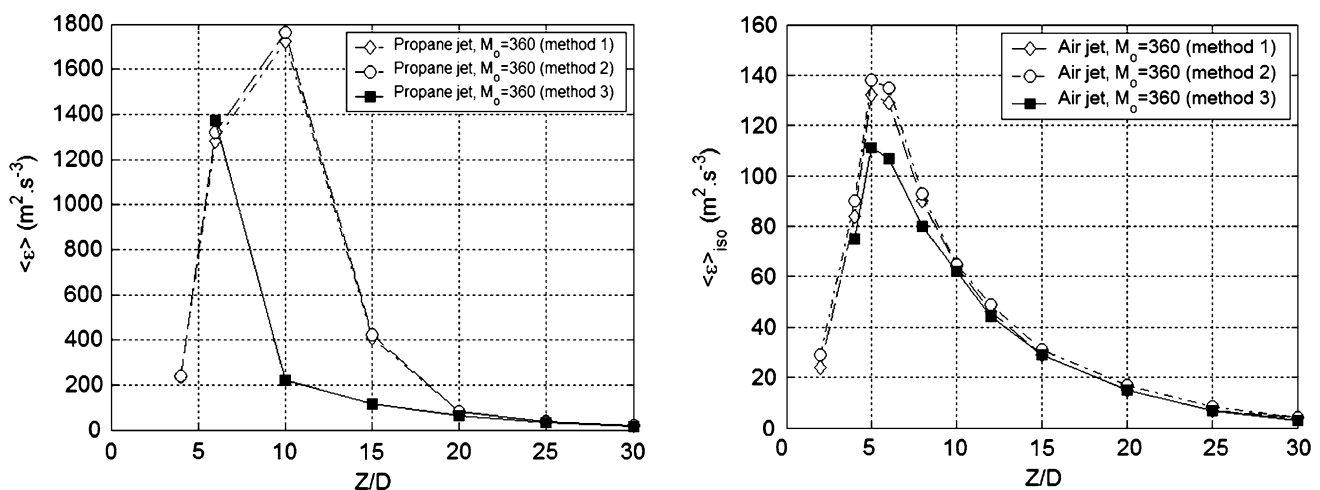


Fig. 10 Isotropic estimates of mean energy dissipation rate $\langle \varepsilon \rangle_{iso}$ ($\text{m}^2 \text{ s}^{-3}$) from Eq. 25, 27 and 28, for the propane jet (left) and air jet (right)

where $\langle q^2 \rangle \equiv \langle u^2 \rangle + \langle v^2 \rangle + \langle w^2 \rangle$. This is “the method 3”. The quantity $d\langle u^2 \rangle/dZ$ in Eq. 28 is deduced from the derivative of the best least-square fitting the axial decreasing law of $\langle u^2 \rangle$.

Figure (10) illustrates the fact that both methods 1 and 2 lead to very nearly the same estimate of $\langle \varepsilon \rangle$, for both air and propane jet, meaning that the velocity spectra are well resolved. Figure (10, right) shows that for the air jet the “method 3” converges to the results given by the other two methods beyond $Z/D \sim 10$ (after the “Near-Field” region emphasized in Fig. 9), most likely because in that part of the flow, isotropy assumption becomes more realistic. Actually, the three methods hinge upon isotropy hypothesis: a local isotropy for methods (1) and (2) and a global isotropy for the third method.

As far as the propane–(air–neon) mixture is concerned, Fig. (10, left) reveals that (1) the absolute value of the dissipation rate $\langle \varepsilon \rangle$ for propane jet is very higher than that for air jet, and that (2) its longitudinal magnitude decreases faster than that of the air jet. Both points (1) and (2) can be attributed to the viscosity gradients effects. For the propane jet, discrepancies among methods 1 (or 2) and 3 are first attributed to the fact that, in the early stage of the mixing, the dissipation is not yet independent of viscosity values, and therefore strong correlations among local viscosity fluctuations and local velocity fluctuations are very probable, leading to the inadequacy of methods 1 and 2 in the early stage of this variable-viscosity flow. Therefore, the most reliable method of inferring $\langle \varepsilon \rangle$ is the method 3, albeit based on a global isotropy assumption. Good agreement between the three methods is revealed at $Z/D = 20$, where $\langle \varepsilon \rangle$ becomes independent of the viscosity. The integral length scales L_1 are estimated from the integral time scale T_1 , viz.

$$L_1 = \langle U \rangle T_1 = \langle U \rangle \int_0^\infty R(\tau) d\tau, \tag{29}$$

with

$$R(\tau) = \frac{\langle u(t)u(t+\tau) \rangle}{\sqrt{\langle u^2(t) \rangle} \sqrt{\langle u^2(t+\tau) \rangle}}. \tag{30}$$

The Taylor micro-scale $\lambda_T = [\langle U_c \rangle^2 \langle u^2 \rangle / \langle (\partial u / \partial t)^2 \rangle]^{1/2}$ and the Kolmogorov micro-scale $\lambda_K = [\langle v_c \rangle^3 / \langle \varepsilon \rangle_{iso}]^{1/4}$ are provided in Table 4, respectively, for air and propane jet discharging into 30% air–70% neon, for the same initial conditions. It is a noteworthy fact that the both integral and Kolmogorov scales are smaller for the propane jet than those of the air jet.

Figure 11 shows the variation of the Reynolds number (based on the Taylor micro-scale, the longitudinal velocity RMS and the local mean viscosity), R_λ , versus the

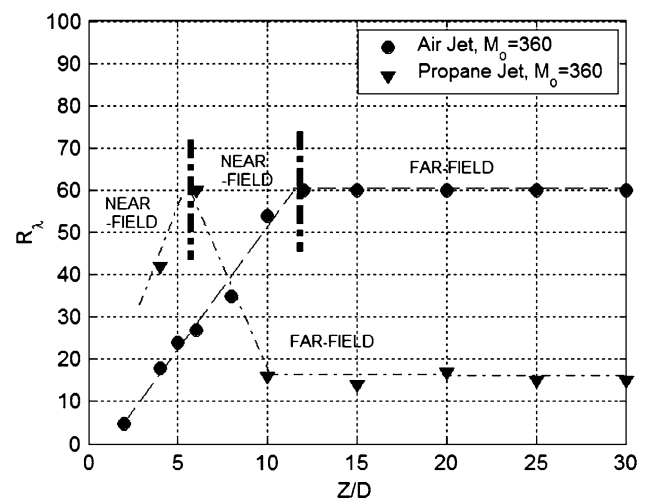


Fig. 11 Evolution of the local Reynolds number R_λ versus Z/D , for propane and air jets at the same initial momentum $M_0 = 360$

downstream location Z/D . After an initial evolution, R_λ becomes nearly constant, at the values of 60 and 15 for air and propane jets, respectively. It is, therefore, clear that the local Reynolds number is drastically reduced in the propane jet by the viscosity gradients, for the same initial jet momentum flux per unit area.

The ratios L_1/λ_K and L_1/λ_T are presented on Fig. 12 for propane and air jets. For the air jet, these ratios strongly vary with Z/D for the range where R_λ is not constant. After R_λ becomes constant (equal to 60), L_1/λ_K and L_1/λ_T are equal to 80 and 10, respectively. In the propane jet, after R_λ becomes constant (equal to 15), these ratios are ~ 18 and ~ 2 , respectively. It is, therefore, clear that the viscosity gradients have a significant effect on the large scales turbulent structures, inducing a drastic decrease in these length scales and of their ratio, in comparison with a flow field with constant viscosity. More generally, the constant-viscosity flow (air jet) exhibits a wider range of scales than the variable-viscosity flow (propane jet), for all the downstream positions. The high viscosity gradients in the latter case accelerate the kinetic energy dissipation and reduce the correlation length as well as the range of scales in the kinetic energy cascade. This property is better illustrated when investigating turbulence spectra.

5.2 Velocity and scalar spectra along the jet axis

The 1D spectra $E_{11}(k_1)$ for the streamwise velocity, respectively, consistent with (Antonia and Orlandi 2003): $\langle u^2 \rangle = \int E_{11}(k_1) dk_1$ are investigated along the jet axis for $Z/D = 15$ and 30 for the air jet at $M_0 = 360 \text{ kg m}^{-1} \text{ s}^{-2}$) discharging into quiescent air (Fig. 13, left) and for the propane jet at $M_0 = 360 \text{ kg m}^{-1} \text{ s}^{-2}$) discharging into air–neon mixture (Fig. 13, right). The spectra are represented as functions of the streamwise wavenumber k_1 and

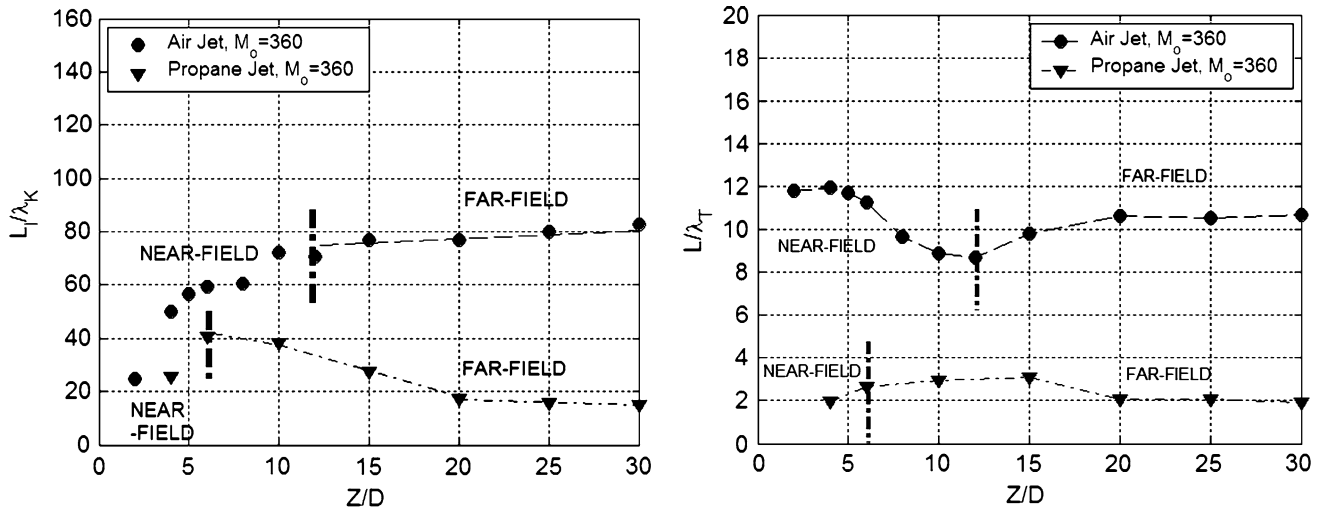


Fig. 12 Left: ratios of integral and Kolmogorov scales along the jet axis versus the downstream location Z/D . Right: ratios of integral and Taylor scales versus the downstream position Z/D . Vertical dash-dotted lines indicate the end of the near-field

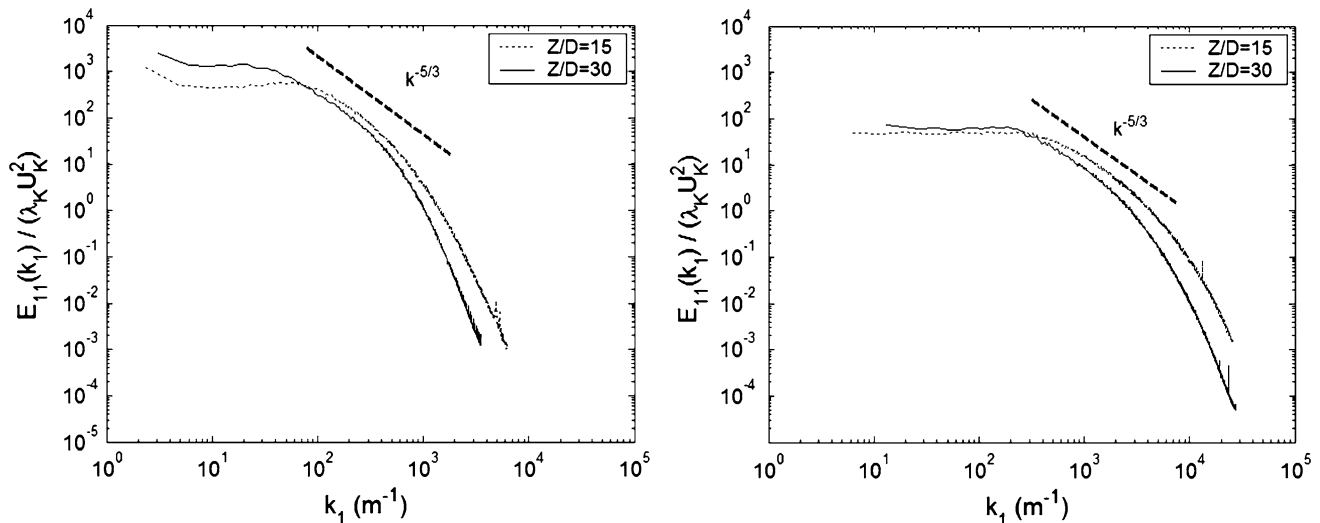


Fig. 13 Normalized velocity spectra $E_{11}(k_1)/\lambda_K U_K^2$ for $Z/D = 15$ and 30 along the jet axis at $M_o = 360$, for air jet at $R_\lambda = 60$ (left) and propane jet at $R_\lambda = 15$ (right)

normalized by the Kolmogorov velocity $U_K = [\langle \varepsilon \rangle_{iso} / \nu_c]^{1/4}$ and Kolmogorov micro-scale λ_K .

Energy spectra for the air jet along the downstream position in the near field exhibit a ‘ $-5/3$ ’ scaling range, with a slightly increasing width from ~ 0.3 decade at $Z/D = 15$ to ~ 0.6 decade at $Z/D = 30$. Although for the propane jet such a ‘ $-5/3$ ’ region is also visible (Fig. 13-right), the extent of this region decreases from ~ 0.4 to ~ 0.2 decade between $Z/D = 15$ and $Z/D = 30$. This particularly narrow ‘ $-5/3$ ’ scaling range in the latter case is attributed to the reinforced kinetic energy dissipation due to the viscosity increase. This is related to the fact that the dissipative length scales for the propane jet are localized at a wavenumber k_d beyond those for the air jet.

Moreover, the number of scales involved in the flow is drastically diminished, a result also emphasized by (Lee et al. 2008) for mixing of variable-viscosity fluids. An analysis of the third-order velocity structure functions would be more indicated for properly addressing the question of the intensity of the energy cascade for this variable-viscosity turbulence. This is the object of future work.

The normalized scalar spectra $\phi(k_1) \langle v_c \rangle / [\langle \varepsilon_s \rangle_{iso} \lambda_K^3]$ are illustrated on Fig. 14 for the downstream positions varying from $Z/D = 4$ – 25 , where the scalar variance dissipation rate is estimated with $\langle \varepsilon_s \rangle_{iso} = -d \langle y_i^2 \rangle / dt = 6 D_{C_3H_8-oxidizer} \int [k_1^2 \phi(k_1)] dk_1$, with $D_{C_3H_8-oxidizer}$ the molecular diffusion coefficient of propane into oxidizer. The

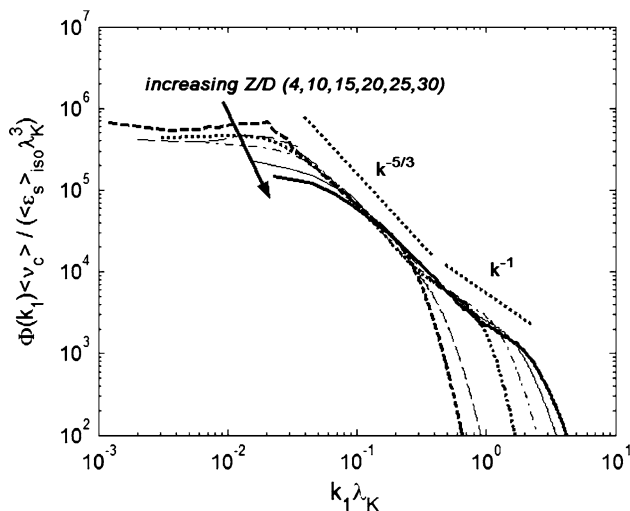


Fig. 14 Scalar spectra along the jet axis for $Z/D = 4$ to $Z/D = 25$ for the propane jet at $M_o = 360$ discharging into air–neon mixture

spectra are represented as functions of the dimensionless streamwise wave number $k_1 \lambda_K = 2\pi f l \langle U_c \rangle \lambda_K$.

Considering that the molecular diffusivity variations do not exceed a few percents, whatever the concentration in a mixture of gases (Hirschfelder et al. 1966), and since the Schmidt number is defined as $Sc = \langle v_c \rangle / D_{C_3H_8-oxidizer}$ (where $\langle v_c \rangle$ is the average viscosity), the viscosity variation involves a Sc variation of the same order, on the jet axis.

From a quantitative viewpoint, the local kinematic viscosity is increasing by a factor of 5.5 along the jet axis from $Z/D = 4$ to $Z/D = 30$, and, therefore, the local Sc number is increasing from $Sc = 1.36$ at $Z/D = 4$ (calculated with the propane viscosity and the molecular diffusion coefficient of the propane–air mixture) to $Sc = 7.5$ at $Z/D = 30$ (calculated with the local viscosity of air–neon mixture and the molecular diffusion coefficient of the propane–air mixture).

Batchelor (1959) indicated that the scalar mixing at $Sc > 1$ is characterized by a viscous-convective range where $\phi(k_1)$ follows a k_1^{-1} power law for the wavenumbers corresponding to the scales between Kolmogorov and Batchelor scale λ_β , where $\lambda_\beta = [\langle \varepsilon \rangle / (\langle v_c \rangle D_{C_3H_8-oxidizer}^2)]^{-1/4} = Sc^{-1/2} \lambda_K$.

As a consequence, a viscous-convective range with a $\sim k_1^{-1}$ slope (Batchelor 1959; Brethouwer et al. 2003; Chakravarthy and Menon 2001) is more and more present beyond the Kolmogorov scale of the velocity field (i.e. at $k_1 \lambda_K > 1$), as the downstream location is increasing. This Batchelor regime is not present at the downstream positions $Z/D = 4$ and 6. Starting with $Z/D = 10$, the Batchelor regime begins to develop and reaches almost one decade at $Z/D = 25$ and 30. A wide scaling range with a ‘ $-5/3$ ’ slope

can also be distinguished for the scalar spectra, in agreement with the Kolmogorov–Obukhov–Corrsin theory, which does not depend on the local Schmidt number. Note also that the extent of this restricted scaling range is much wider than that exhibited by the velocity spectra, a result that is in full agreement with the results discussed in the existing literature, e.g. (Shraiman and Siggia 2000).

6 Conclusions

We have developed and validated an innovative reliable technique for measuring velocity fluctuations independently of concentration measurements (by Rayleigh light scattering), in a turbulent propane jet discharging into quiescent air. By adding a small amount of neon to the surrounding air, we showed both analytically and experimentally that the hot-wire response becomes insensitive to the concentration of the field. As a result, the hot-wire calibration curve for this propane–(air–neon) mixture is quasi-unique and is not dependent on the local concentration. This is the main result reported in this paper.

Advantages of this velocity measurement technique are

- Independence of the velocity and scalar (concentration of fuel) measurements. Since the hot-wire response is sensitive to both local concentration and velocity, we have demonstrated that the velocity can be measured independently of the Rayleigh signal by replacing a fraction of air by neon. Velocity fluctuation measurements performed using this technique have a maximal relative error of 15% over the range 0–10 m s⁻¹.
- The use of neon is particularly interesting because of its neutral chemical impact on a reacting flow. It could therefore be subsequently used for a study of a reacting flow having similar dynamics as that of the non-reacting flow.

Although not required to make the velocity measurements, Rayleigh light scattering was used to infer the local (fluctuating) concentration, and, therefore, the viscosity of the fluid. It was demonstrated that the propane–(air–neon) mixture might be considered as a binary fluid for RLS measurements, to a good approximation.

Velocity and concentration measurements were performed in a turbulent propane jet discharging into an air–neon co-flow, for which the densities and viscosities ratios are of 1.52 and 1/5.5, respectively. These measurements were first validated: the axial decay of the mean velocity and concentration, as well as the lateral mean and RMS profiles of velocity and concentration, are in full agreement with the existing literature.

A further characterization of the variable-viscosity flow along the axis of the round jet was performed. This

variable-viscosity flow was compared with a turbulent air jet discharging into still air. We have chosen to compare the same flow (round jet) with two different fluids: pure air and C_3H_8 -(air–neon). Both flows had the same initial jet momentum (the same initial Reynolds number being irrelevant for such variable density/viscosity flows). For the case of the propane jet, the viscosity of the fluid increases rapidly with increasing downstream position and exhibits properties different of those of the classical air jet. Some particular properties of the propane jet were

- increased values of the turbulence intensity (24%, compared to 15% for the air jet) and an early self-similarity, since $Z/D = 8$;
- a higher mean kinetic energy dissipation rate along the jet axis (by up to a factor of 13), and a more rapid decay of this quantity;
- a reduction in both the integral and Kolmogorov scales, as well as of their ratio;
- a reduction (by up to a factor of 4) of the local Reynolds number (based on the Taylor microscale);
- a diminished width of the ‘ $-5/3$ ’ scaling range of the velocity spectra;
- the appearance of a Batchelor regime with a ‘ -1 ’ scaling law (viscous-convective range) on the scalar spectrum, as the local Schmidt number increased from 1.36 to 7.5 for farther downstream locations.

This work provides more insight into turbulent mixing with non-constant-viscosity flow fields. The velocity measurement technique proposed herein provides an accurate means to study turbulent flows with variable viscosity and could be applied to other gas mixtures. In the combustion context, the present work provides insight on the micro-mixing of a fuel-oxidizer mixture to improve non-premixed combustion modeling.

Note that by adding neon to the air helps in properly characterizing the velocity field in this new mixture. However, to obtain the details of the unmodified mixing (propane–pure air for instance, which has different viscosity variations), analytical work is required by taking into account the Reynolds number influence on the spectra (or any other statistics). Models for the spectra are to be investigated, adapted and eventually used.

We lastly comment on some of the hypotheses used in inferring the mean energy dissipation rate in variable-viscosity flows. In this paper, this quantity was expressed:

- By the 1-point energy budget, since its physical significance is based on the rate at which kinetic energy is destroyed. With the hypothesis that isotropy is locally respected when mixing is more and more effective (Lee et al. 2008), the production term in the kinetic energy balance equation becomes increasingly negligible, and

the expression of the mean energy dissipation rate reduces to the decay of the total kinetic energy. This only holds on the jet axis.

- Using classical expressions (Eq. 25) in which the mean value of the kinematic viscosity is used. This is correct only if the mean value of the dissipation rate becomes, somewhere downstream the injection of the two variable-viscosity streams, independent of the viscosity, and, therefore, independent of the location where the estimate of dissipation rate is made. A recent work (Lee et al. 2008) proves, using DNS, that the energy dissipation rate does indeed become (rapidly) independent of the local viscosity of the flow. This is a significant result in the context of our work, which allows us also to express the dissipation rate using Eq. 25 at some distance downstream the injection. Further investigations are necessary to *a priori* clarify this distance, according to the flow type and mixing.

Finally, we remark that further analysis is necessary to better understand the physical mechanisms that govern this variable-viscosity turbulence. The Navier–Stokes equations describing these particular variable-viscosity flows require the knowledge of joint velocity-viscosity statistics knowledge, i.e. joint velocity-scalar statistics. These joint statistics could be provided, for example, by our technique because of its high spatial resolution offered by the 800 μm of separation between the hot wire and the Rayleigh probe volumes.

Acknowledgments Financial support of ANR ‘Agence Nationale de la Recherche’ under the activity ANR 05-BLAN-0242-02 ‘Micromélange’ is gratefully acknowledged.

References

- Amielh M, Djeridane T, Anselmet F, Fulachier L (1996) Velocity near-field of variable density turbulent jets. *Int J Heat Mass Transf* 39(10):2149–2164
- Antonia RA, Orlandi P (2003) Effect of Schmidt number on small-scale passive scalar turbulence. *Appl Mech Rev* 56(6):615–632
- Baccaglini G, Kassoy DR, Libby PA (1969) Heat transfer to cylinders in nitrogen-helium and nitrogen neon mixtures. *Phys Fluids* 12(7):1378–1381
- Batchelor GK (1959) Small-scale variation of convected quantities like temperature in turbulent fluid. Part 1. General discussion and the case of small conductivity. *J Fluid Mech* 5:113–133
- Becker HA, Hottel HC, Williams GC (1967) The nozzle-fluid concentration field of the round, turbulent, free jet. *J Fluid Mech* 30:285–301
- Birch AD, Brown DR, Dodson MD, Thomas JR (1978) Turbulent concentration field of a methane jet. *J Fluid Mech* 88:431–449
- Boersma BJ, Brethouwer G, Nieuwstadt FTM (1998) A numerical investigation on the effect of the inflow conditions on the self-similar region of a round jet. *Phys Fluids* 10(4):899–909
- Brethouwer G, Hunt JCR, Nieuwstadt FTM (2003) Micro-structure and lagrangian statistics of the scalar field with a mean gradient in isotropic turbulence. *J Fluid Mech* 474:193–225

- Chakravarthy VK, Menon S (2001) Linear eddy simulations of Reynolds number and Schmidt number effects on turbulent scalar mixing. *Phys Fluids* 13(2):488–499
- Chassaing P (1979) Mélange turbulent de gaz inertes dans un jet de tube libre, Thèse Doc. Es Science, INP Toulouse, No. 42
- Chassaing P, Harran G, Joly L (1994) Density fluctuation correlations in free turbulent binary mixing. *J Fluid Mech* 279:239–278
- Chen CJ, Rodi W (1980) Vertical turbulent buoyant jets, a review of experimental data, Pergamon
- Dahm WJA, Dimotakis PE (1987) Measurements of entrainment and mixing in turbulent jets. *AIAA J* 25:1216–1223
- Dibble RW, Hartmann V, Schefer RW, Kollmann W (1987) Conditional sampling of velocity and scalars in turbulent flames using simultaneous LDV-Raman scattering. *Exp Fluids* 5(2):103–113
- Djeridane T, Amielh M, Anselmet F, Fulachier L (1996) Velocity near-field of variable density turbulent jets. *Phys Fluids* 8(6):1614–1630
- Dowling DR, Dimotakis PE (1990) Similarity of the concentration field of gas-phase turbulent jets. *J Fluid Mech* 218:109–141
- Era Y (1993) Simultaneous measurement of concentration and velocity by applying hot-wire techniques. *Heat Transf* 22(1):14–27
- Feng H, Olsen M, Fox RO, Hill JC (2007) Conditional statistics of passive-scalar mixing in a confined wake flow. *Exp Fluids* 42(6):847–862
- Fernandez-Tarrazo E, Vera M, Linan A (2006) Liftoff and blowoff of a diffusion flame between parallel streams of fuel and air. *Comb Flame* 144:261–276
- Graham SC, Grant AJ, Jones JM (1974) Transient molecular concentration measurements in turbulent flows using Rayleigh light scattering. *AIAA J* 12:1140–1142
- Gustavsson JPR, Segal C (2005) Filtered Rayleigh scattering velocimetry-accuracy investigation in a $M = 2.2$ axisymmetric jet. *Exp Fluids* 38(1):11–20
- Hermanns M, Vera M, Linan A (2007) On the dynamics of flame edges in diffusion-flame/vortex interactions. *Comb Flame* 149:32–48
- Hirschfelder JO, Curtiss CF, Bird RB (1966) Molecular theory of gases and liquids. John Wiley, New York
- Lavoie P, Avallone G, De Gregorio F, Romano GP, Antonia RA (2007) Spatial resolution of PIV for the measurement of turbulence. *Exp Fluids* 43(1):39–51
- Lee K, Girimaji SS, Kerimo J (2008) Validity of Taylor's dissipation-viscosity independence postulate in variable-viscosity turbulent fluid mixtures. *Phys Rev Lett* 101:074501
- Lemoine F, Antoine Y, Wolff M, Lebouche M (1999) Simultaneous temperature and 2D velocity measurements in a turbulent heated jet using combined laser-induced fluorescence and LDA. *Exp Fluids* 26(4):315–323
- Lide D (2007–2008) Handbook of Chemistry and Physics, 88th edn. CRC Press
- Lockwood FC, Moneib HA (1980) Fluctuating temperature measurements in a heated round free jet. *Comb Sci Technol* 22:63–71
- Lubbers CL, Brethouwer G, Boersma BJ (2001) Simulation of the mixing of a passive scalar in a round turbulent jet. *Fluid Dyn Res* 28(3):189–208
- Miller PL, Dimotakis PE (1996) Measurements of scalar power spectra in high Schmidt number turbulent jets. *J Fluid Mech* 308:129–146
- Nelkin M (2000) Turbulence in fluids. *Am J Phys* 68(4):310–318
- Panchapakesan NR, Lumley JL (1993) Turbulence measurements in axisymmetric jets of air and helium. Part 1. Air jet. *J Fluid Mech* 246:197–223
- Pao YH (1965) Structure of turbulent velocity and scalar fields at large wave numbers. *Phys Fluids* 8:1063–1075
- Papanicolaou PN, List EJ (1988) Investigations of round vertical turbulent buoyant jets. *J Fluid Mech* 195:341–391
- Pitts WM, Kashiwagi T (1984) The application of laser-induced Rayleigh light scattering to the study of turbulent mixing. *J Fluid Mech* 141:391–429
- Pitts WM, McCaffrey BJ (1986) Response behaviour of hot wires and films to flows of different gases. *J Fluid Mech* 169:465–512
- Pitts WM, McCaffrey BJ, Kashiwagi T (1983) New diagnostic technique for simultaneous time-resolved measurements of concentration and velocity in simple turbulent flow systems. In: Proceedings of the 4th symposium on Turbulent Shear Flows, Karlsruhe, A85-14326-04-34, F.R. Germany
- Pollock CR (1994) Fundamentals of optoelectronics. Irwin Chicago, Hardcover
- Richardson CD, Pitts WM (1993) Global density effects on the self-preservation behaviour of turbulent free jets. *J Fluid Mech* 254:417–435
- Ruffin E, Schiestel R, Anselmet F, Amielh M, Fulachier L (1994) Investigation of characteristic scales in variable density turbulent jets with a second-order model. *Phys Fluids* 6:2785–2799
- Sakai Y, Watanabe T, Kamohara S, Kushida T, Nakamura I (2001) Simultaneous measurements of concentration and velocity in a CO_2 jet issuing into a grid turbulence by two-sensor hot-wire probe. *Int J Heat Fluid Flow* 22:227–236
- Schefer RW, Dibble RW (1986) Rayleigh scattering measurements of mixture fraction in a turbulent nonreacting propane jet. *AIAA J* 23(7):1070–1078
- Shardanand, Prasad Rao AD (1977) Absolute Rayleigh scattering cross-sections of gases and freons of stratospheric interest in the visible and ultraviolet regions, *NASA TN D-8442*, National Aeronautics and Space Administration, Washington D.C
- Shraiman BI, Siggia ED (2000) Scalar turbulence. *Nature* (review) 405:639–646
- Sreenivasan KR (1984) On the scaling of the turbulence energy dissipation rate. *Phys Fluids* 27:1048–1051
- Su LK, Mungal MG (2004) Simultaneous measurement of scalar and velocity field evolution in turbulent crossflowing jets. *J Fluid Mech* 513:1–45
- Sutton JA, Driscoll JF (2004) Rayleigh scattering cross-sections of combustion species at 266, 355 and 532 nm for thermometry applications. *Opt Lett* 29(22):2620–2622
- Thring MW, Newby MP (1952) Combustion length of enclosed turbulent jet flames, In: 4th international symposium on combustion, The Combustion Institute, Baltimore, pp 789–796
- Warnatz J (1981) The structure of laminar alkane-, alkene-, and acetylene flames, In: 18th international symposium on combustion, The Combustion Institute, pp 369–384
- Way J, Libby PA (1971) Application to hot-wire anemometry and digital techniques to measurements in a turbulent helium jet. *AIAA J* 9:1567–1573
- Wu P, Libby PA (1971) Heat transfer to cylinders in helium and helium-air mixtures. *Int J Heat Mass Transf* 14:1071–1077
- Zhao FQ, Hiroyasu H (1993) The applications of laser Rayleigh light scattering to combustion diagnostics. *Prog Energy Comb Sci* 19:447–485